Physics-Informed Neural Networks with good lattice points set for solve low regularity PDEs and high dimensional PDE*

Yu Yang^a, PingAn He^b, Xiaoling Peng^{c,*} and Qiaolin He^{a,*}

ARTICLE INFO

Keywords: deep learning neural networks partial differential equation sampling good lattice points.

ABSTRACT

When dealing with a large number of points was required, the traditional uniform sampling approach for approximating integrals using the Monte Carlo method becomes inefficient. In this work, we leverage the good lattice point sets from number-theoretic methods for sampling purposes and develop a deep learning framework that integrates the good lattice point sets with Physics-Informed Neural Networks. This framework is designed to address low-regularity and high-dimensional problems. Furthermore, rigorous mathematical proofs are provided for our algorithm, demonstrating its validity. Lastly, in the experimental section, we employ numerical experiments involving the Poisson equation with low regularity, the two-dimensional inverse Helmholtz equation, and high-dimensional linear and nonlinear problems to illustrate the effectiveness of our algorithm from a numerical perspective.

1. Introduction

Numerically solving partial differential equations (PDEs) [19] has always been one of the concerns of frontier research. In recent years, as the computational efficiency of hardware continues to improve, solving PDEs using deep learning has gradually come into people's view. Based on the control equations and boundary conditions of PDEs, Physics-Informed Neural Networks and Deep Galerkin method were developed in [18] and [22]; based on the variational form of PDEs, Deep Ritz method was developed in [26]; based on stochastic differential equations, deep BSDE framework was developed in [4], which is good at solving high-dimensional PDEs; and from the perspective of operator learning, [12] and [10] developed the deep operator networks (DeepONet) and the Fourier Neural Operator framework (FNO). In this paper, we are concerned with Physics-Informed Neural Networks (PINN).

Here, we first briefly introduce PINN, and a detailed introduction can be found in Section 2.2. For a general PINN, its network structure is a common fully connected neural network, its input is the sampling points inside the computational region, and its output is the predicted solution of the system of partial differential equations. The form of its loss function is usually chosen to be based on the L2 norm, which mainly contains the residual loss based on the partial differential control equations, the boundary loss based on the boundary conditions, and more relevant physical constraints. Then, during the training process, the value of the loss function is reduced by an optimization algorithm while updating the parameters of the neural network. In the ideal situation, that is, after the optimization algorithm finds the global minimum of the loss function, then the training of the PINN is stopped, at which point the predicted solution output by the neural network is considered to be an approximation of the true solution of the system of partial differential equations. At present, it is a widely accepted fact that the error of PINN is composed of three components which are approximation error, estimation error and optimization error. In short, the reason for the approximation error is that the space in which the true solution actually exists is different from the space represented by the neural network. This error is mainly determined by the structure and size of the neural network as well as the activation function. And the estimation error is due to the Monte Carlo (MC) method to discretize the loss function. As for the optimization error, it arises from the inability of the optimization algorithm to find the global minimum point of the loss function.

ORCID(s): 0009-0005-1428-6745 (Y. Yang)

^aSchool of Mathematics, Sichuan University, 610065, Chengdu, China.

^b Faculty of Science and Technology, BNU-HKBU United International College, 519087, Zhuhai, China.

^cGuangdong Provincial Key Laboratory of Interdisciplinary Research and Application for Data Science, BNU-HKBU United International College, 519087, Zhuhai, China

^{*}This research is partially sponsored by the National key R & D Program of China (No.2022YFE03040002) and the National Natural Science Foundation of China (No.11971020, No.12371434).

yangyu1@stu.scu.edu.cn (Y. Yang); t330202702@mail.uic.edu.cn (P. He); xlpeng@uic.edu.cn (X. Peng); qlhejenny@scu.edu.cn (Q. He)

The main focus of this paper is on the estimation error, and our goal is to improve the prediction performance of PINN by reducing the estimation error. When using MC methods to discretize the loss function in integral form, sampling points obeying a uniform distribution are usually sampled to serve as empirical losses. It is then worth considering how to get better sampling points. Sampling methods are mainly categorized into non-uniform adaptive sampling and uniform non-adaptive sampling. Currently, there have been many works on non-uniform adaptive sampling. Lu et al. in their work [13], introduced the residual-based adaptive refinement (RAR) method aimed at enhancing the training efficiency of PINN. Specifically, this method adaptively adds training points in regions where the residual loss is large. In [27], a novel residual-based adaptive distribution (RAD) method is proposed. The core concept of this method involves constructing a probability density function that relies on residual information and subsequently employing adaptive sampling techniques in accordance with this density function. Tang et al., as detailed in [25], presented an adaptive sampling framework for solving PDEs. This framework takes a approach by focusing on the variance of the residual loss and leveraging KRNet, as introduced in [24], to facilitate the process. Contrary to the aforementioned methods that rely on residual loss, Yang et al. introduced an MMPDE-Net grounded in the moving mesh method in [29], which cleverly harnesses information from the solution to devise a monitor function, facilitating adaptive sampling of the training points.

However, not much work has been done on uniform non-adaptive sampling. Compared to non-uniform adaptive sampling, uniform non-adaptive sampling does not require a pre-training step to obtain information about the loss function or the solution, which directly improves efficiency. There are several common methods of uniform non-adaptive sampling, which include 1) equispaced uniform points sampling, a method that uniformly selects points from an array of evenly spaced points, frequently employed in addressing low-dimensional problems; 2) Latin hypercube sampling ([23]), which is a stratified sampling method based on multivariate parameter distributions; 3) uniformly random sampling, which draws points at random in accordance with a continuous uniform distribution within the computational domain, representing the most widely adopted method.

In this paper, we focus our sampling methods on number-theoretic methods (NTM). NTM was created by Korobov [8]. It is a method based on number theory to produce uniformly distributed points, which is used to reduce the need for sampling points when calculating numerical integrals. Later on, researchers found that the NTM and the MC method share some commonalities in terms of uniform sampling, so it is also known as the quasi-Monte Carlo (QMC) method. In NTM, there are several types of sampling points, such as Halton sequences, Hammersley sequences, Sobol sequences and good lattice points set. Among them, we are mainly concerned with the good lattice points set (GLP set). It is well known that the MC method approximates the integral with an error of $O(N^{-\frac{1}{2}})$ when discretizing the integral using N i.i.d random points. Again using N points (deterministic), the NTM method approximates the integral with an error of $O(\frac{(\log N)^d}{N})$, where d is the dimension of the integral (see Lemma 1). Thus, with the same accuracy, NTM can greatly reduce the number of points to be sampled. When using PINN to solve some partial differential equations, a large number of sampling points is required, such as low regularity problems or high dimensional problems. When using PINN to solve some partial differential equations, a large number of sampling points is required, such as low regularity problems or high dimensional problems. In this case, the usual uniform random sampling is very inefficient. In this paper, for low regularity problems and high dimensional problems, GLP sampling is sampled instead of uniform random sampling, which not only reduces the consumption of computational resources, but also improves the accuracy. Meanwhile, we also give an upper bound on the error of the predicted solution of PINN when using GLP sampling through rigorous mathematical proofs. And according to the error upper bound, we also prove that GLP sampling is more effective than uniform random sampling.

The rest of the paper is organized as follows. In Section 2, we will go into more detail about PINN and its loss function. In Section 3, we will describe GLP sampling in detail and also give the neural network framework incorporating GLP sampling and give the error estimates. Numerical experiments are shown in Section 4 to verify the effectiveness of our method. Finally, conclusions are given in Section 5.

2. Preliminary Work

2.1. Problem formulation

The general formulation of the partial differential equation problem we are considering is as outlined below

$$\begin{cases} A[u(x)] = f(x), & x \in \Omega, \\ B[u(x)] = g(x), & x \in \partial\Omega. \end{cases}$$
 (1)

Here, $\Omega \subset \mathbb{R}^d$ represents a bounded, open, and connected domain which surrounded by a polygonal boundary $\partial\Omega$. And u(x) is the unique solution to this problemm. There are two partial differential operators \mathcal{A} and \mathcal{B} defined in Ω and on $\partial\Omega$. Additionally, f(x) serves as the source function within Ω and g(x) represents the boundary conditions on $\partial\Omega$.

2.2. Introduction to PINN

As we mentioned in Section 1, for a general PINN, its input consists of sampling points x located within the domain Ω or on its boundary $\partial\Omega$, and its output is the predicted solution $u(x;\theta)$. Here, θ represents the parameters of the neural network, typically comprising weights and biases. Suppose that $A[u(x;\theta)] - f(x) \in L^2(\Omega)$ and $B[u(x;\theta)] - g(x) \in L^2(\partial\Omega)$, the loss function of PINN can be expressed as

$$\mathcal{L}(\boldsymbol{x};\theta) = \alpha_{1} \|\mathcal{A}[\boldsymbol{u}(\boldsymbol{x};\theta)] - f(\boldsymbol{x})\|_{2,\Omega}^{2} + \alpha_{2} \|\mathcal{B}[\boldsymbol{u}(\boldsymbol{x};\theta)] - g(\boldsymbol{x})\|_{2,\partial\Omega}^{2}$$

$$= \alpha_{1} \int_{\Omega} |\mathcal{A}[\boldsymbol{u}(\boldsymbol{x};\theta)] - f(\boldsymbol{x})|^{2} d\boldsymbol{x} + \alpha_{2} \int_{\partial\Omega} |\mathcal{B}[\boldsymbol{u}(\boldsymbol{x};\theta)] - g(\boldsymbol{x})|^{2} d\boldsymbol{x}$$

$$\triangleq \alpha_{1} \int_{\Omega} |r(\boldsymbol{x};\theta)|^{2} d\boldsymbol{x} + \alpha_{2} \int_{\partial\Omega} |b(\boldsymbol{x};\theta)|^{2} d\boldsymbol{x},$$

$$\triangleq \alpha_{1} \mathcal{L}_{r}(\boldsymbol{x};\theta) + \alpha_{2} \mathcal{L}_{b}(\boldsymbol{x};\theta)$$
(2)

where α_1 is the weight of the residual loss $\mathcal{L}_r(x;\theta)$ and α_2 is the weight of the boundary loss $\mathcal{L}_b(x;\theta)$. We now use the residual loss $\mathcal{L}_r(x;\theta)$ as an example of how to discretize by Monte Carlo methods.

$$\mathcal{L}_{r}(\boldsymbol{x};\theta) = \int_{\Omega} |r(\boldsymbol{x};\theta)|^{2} d\boldsymbol{x} = V(\Omega) \int_{\Omega} |r(\boldsymbol{x};\theta)|^{2} U(\Omega) d\boldsymbol{x}$$

$$= V(\Omega) \mathbb{E}_{\boldsymbol{x} \sim U}(|r(\boldsymbol{x};\theta)|^{2})$$

$$\approx V(\Omega) \frac{1}{N_{r}} \sum_{i=1}^{N_{r}} |r(\boldsymbol{x}_{i};\theta)|^{2}, \quad \boldsymbol{x} \sim U(\Omega)$$
(3)

where V is the volume, U is the uniform distribution, and \mathbb{E} is the mathematical expectation. Thus, after we sample uniformly distributed residual training points $\{x_i\}_{i=1}^{N_r} \subset \Omega$ and boundary training points $\{x_i\}_{i=1}^{N_b} \subset \partial \Omega$, we can write the following the empirical loss,

$$\mathcal{L}_{N}(\mathbf{x};\theta) = \frac{\alpha_{1}V(\Omega)}{N_{r}} \sum_{i=1}^{N_{r}} |r(\mathbf{x}_{i};\theta)|^{2} + \frac{\alpha_{2}V(\Omega)}{N_{b}} \sum_{i=1}^{N_{b}} |b(\mathbf{x}_{i};\theta)|^{2}, \quad N = N_{r} + N_{b}.$$
 (4)

Finally, we usually use gradient descent methods, such as Adam [7] and LBFGS [11], to optimize for empirical loss $\mathcal{L}_N(\mathbf{x};\theta)$. In Algorithm 1, the general form of the stochastic gradient descent method is given. Ideally, $\mathcal{L}_N(\mathbf{x};\theta)$ will keep decreasing and even reach 0. Then, at this point, the approximate solution of the PINN on the training set can be considered to be the same as the true solution. In fact, when the empirical loss is small enough, we consider that the approximate solution already has a small enough error ([20],[21]).

Algorithm 1: The general stochastic gradient descent algorithm

```
Initialize the parameters of neural networks: \theta = \theta_0. Choose the learning rate at each training epochs: \eta_i. for Traning epochs i = 0: M - 1 do

Select a random sample x_i from the training set;

Calculating the gradient g(x_i, \theta_i) = \frac{\partial \mathcal{L}_N((x_i; \theta_i))}{\partial \theta_i};

Update \theta_{i+1} by \theta_{i+1} = \theta_i - \eta_i g(x_i, \theta_i).
```

3. Mainly Work

3.1. Methods

In this section, we will describe our model in detail. First, we will describe how to get good lattice points set.

Consider that our sampling space is unit cube $C^d = [0, 1]^d$, and in fact, after obtaining the good lattice points set on C^d , they can be transferred to other spaces by coordinate transformation. In the following, we will introduce some classical definitions on C^d in the number theoretic methods.

Definition 1. Let $X_N = \{x_i\}_{i=1}^N$ be a collection of points on C^d . For a vector $\gamma \in C^d$, let $K(\gamma, X_N)$ denote the number of points in X_N that satisfy $x_i < \gamma$. Then there are

$$D(N,X) = \sup_{\gamma \in C^d} \left| \frac{K(\gamma, X_N)}{N} - V(|0, \gamma|) \right|$$
 (5)

Call $D(N, X_N)$ the discrepancy of X_N , where $V([0, \gamma])$ denotes the volume of the cube formed by the vector γ from 0.

The discrepancy defined in Definition 1 is an important measure of the uniformity of a point set on the unit cube. For a point set X_N , the smaller its discrepancy, the higher the uniformity of this point set. Based on Definition 1, the definition of lattice points can be introduced.

Definition 2. Let $GV = (N; h_1, h_2, ..., h_s) \in C^d$ to be a vector of integers satisfying $1 \le h_i < N$, $h_i \ne h_j (i \ne j)$, d < N and the greatest common divisor $(N, h_i) = 1, i = 1, ..., d$.Let

$$\begin{cases} q_{ij} \equiv ih_j \pmod{N}, \\ x_{ij} = \frac{2q_{ij} - 1}{2N}, & i = 1, ..., N, j = 1, ..., d \end{cases}$$
(6)

where q_{ij} satisfies $1 \le q_{ij} \le N$. Then the point set $X_N = \{x_i = (x_{i1}, x_{i2}, ..., x_{id}), i = 1, ..., N\}$ is called the set of lattice points of the generating vector GV. And a point set X_N is a good lattice points set if X_N has the minimum discrepancy $D(N, X_N)$ among all possible generating vectors.

Definition 2 not only introduces us to the definition of a good lattice point set, but also tells us that good lattice point set have excellent low discrepancy. In fact, some work has been done by researchers on the error bound about the MC method and the set of good grid points. According to the central limit theorem and the Koksma-Hlawka inequality [5], we can get the following famous lemma (more details can be found in [17]).

Lemma 1. If $f(\mathbf{x}) \in \mathbb{L}_2(\Omega)$: $\Omega = [0, 1]^d \to \mathbb{R}$ has bounded variation in the sense of Hardy and Krause, then there is

$$\int_{\Omega} f^2(\mathbf{x}) d\mathbf{x} \leq \frac{1}{N} \sum_{i=1}^{N} f^2(x_i) + O\left(N^{-\frac{1}{2}}\right), \text{ where } \left\{\mathbf{x}_i\right\}_{i=1}^{N} \text{ is a uniform random points set,}$$

$$\int_{\Omega} f^2(\mathbf{x}) d\mathbf{x} \leq \frac{1}{N} \sum_{i=1}^{N} f^2(x_i) + O\left(\frac{(\log N)^d}{N}\right), \text{ where } \left\{\mathbf{x}_i\right\}_{i=1}^{N} \text{ is a good lattice points set.}$$

Remark 1. According to [5] and [3], a sufficient condition for f to have bounded variance in the Hardy-Krause sense is that f has continuous mixed partial differential derivatives. In fact, some common activation functions in neural networks, such as the hyperbolic tangent function and the Sigmoid function, they are infinite order derivable. Therefore, when the activation functions mentioned above are chosen, the function $r(\mathbf{x}; \theta)$ and $b(\mathbf{x}; \theta)$ induced by the predicted solutions $\mathbf{u}(\mathbf{x}; \theta)$ generated by the PINN also satisfies the conditions of Lemma 1 (similar points can be found in [15].).

Then, according to Definition 2, an ensuing problem is how to choose the appropriate generating vectors for the generation of the set of good lattice points via Eq 6. As early as the last century, this problem has been considered by researchers such as Korobov and Niederreiter ([9],[16]). The method of finding the generating vectors is not unique, and a feasible method is described below. For a lattice point set X_P whose total number is a certain prime number P, the generating vector $GV = (P; 1, g, g^2, ..., g^{d-1})$ is constructed by finding a certain special primitive root g among the

primitive roots modulo P, so that the lattice point set corresponding to GV has the smallest discrepancy. Fortunately, Hua and Wang ([6]) have provided detailed generating vectors corresponding to some good lattice point sets on unit cubes of different dimensions, which eliminates the need for us to calculate the generating vectors from scratch.

Next, after getting the GLP set, we return our attention to the loss function of PINN. Since the boundary loss usually account for a relatively small percentage of the total, and can even be completely equal to 0 by forcing the boundary conditions([14]), we focus on the residual loss in the following. Recalling equation 3, when the computational region $\Omega = C^d$, the discrete residual loss under uniform sampling can be written as

$$\mathcal{L}_r(\boldsymbol{x};\theta) = \int_{\Omega} |r(\boldsymbol{x};\theta)|^2 d\boldsymbol{x} = \mathbb{E}_{\boldsymbol{x} \sim U}(|r(\boldsymbol{x};\theta)|^2) \approx \frac{1}{N_r} \sum_{i=1}^{N_r} |r(x_i;\theta)|^2, \quad \boldsymbol{x} \sim U(\Omega).$$
 (7)

Given a good lattice points set $X_{N_r} = \left\{ \mathbf{x}_i \right\}_{i=1}^{N_r} \subset \Omega$, then there is a discrete residual loss as follows. In notation, this paper uses superscripts to distinguish between sampling methods

$$\mathcal{L}_{r,N_r}^{GLP}(\mathbf{x};\theta) = \frac{1}{N_r} \sum_{i=1}^{N_r} |r(x_i;\theta)|^2, x_i \in X_{N_r}.$$
 (8)

Then according to Eq 4, we have the following loss function.

$$\mathcal{L}_{N}(\boldsymbol{x};\boldsymbol{\theta}) = \alpha_{1} \mathcal{L}_{r,N_{a}}^{GLP}(\boldsymbol{x};\boldsymbol{\theta}) + \alpha_{2} \mathcal{L}_{r,N_{b}}^{UR}(\boldsymbol{x};\boldsymbol{\theta}), \quad N = N_{r} + N_{b}. \tag{9}$$

Finally, we use gradient descent method to optimize the loss function Eq 9. The flow of our approach is summarized in Algorithm 2.

Algorithm 2: Algorithm of PINN based on GLP set

Symbols: Maximum epoch number of PINN training: M; the numbers of total points in $\Omega = C^d$ and $\partial \Omega$: N_r , and N_b ; generating vector: $GV = (N_r; h_1, h_2, ..., h_d)$; uniform boundary training points $\mathcal{X}_{N_b} := \left\{ \mathbf{x}_k \right\}_{k=1}^{N_b} \subset \partial \Omega$; the number of test set points: N_T ; test set $\mathcal{X}_T := \left\{ \mathbf{x}_k \right\}_{k=1}^{N_T} \subset \Omega \cup \partial \Omega$; the

parameters of PINN: θ .

Sampling:

Input generating vector $GV = (N_r; h_1, h_2, ..., h_d)$ for GLP sampling.

$$x_{ij} = \frac{2q_{ij}-1}{2N}$$
, where $q_{ij} \equiv ih_j \pmod{N_r}$, $i = 1, ..., N, j = 1, ..., d$

Get the GLP set
$$\mathcal{X}_{N_r} := \{x_k = (x_{k1}, x_{k2}, ..., x_{kd})\}_{k=1}^{N_r} \subset \Omega$$
.

Training:

Input $\mathcal{X}_{N}^{-} := \mathcal{X}_{N_{n}} \cup \mathcal{X}_{N_{h}}$ into PINN.

Initialize the output $u(\mathcal{X}_N; \theta_0)$.

for
$$i = 0 : M - 1$$
 do

$$\mathcal{L}_{N}\left(\mathcal{X}_{N};\theta_{i}\right) = \alpha_{1}\mathcal{L}_{r,N_{r}}^{GLP}\left(\mathcal{X}_{N_{r}};\theta_{i}\right) + \alpha_{2}\mathcal{L}_{r,N_{b}}^{UR}\left(\mathcal{X}_{N_{b}};\theta_{i}\right);$$

Update θ_{i+1} by descending the gradient of $\mathcal{L}_N(\mathcal{X}_N; \theta_i)$.

end

Testing:

Input test set \mathcal{X}_T into PINN.

Output $u(\mathcal{X}_T; \theta_M)$.

3.2. Error Estimation

We consider the problem Eq (1) and assume that both \mathcal{A} and \mathcal{B} are linear operators. One easily verifiable fact is that whether you use uniform random samplings or good lattice points set based on number-theoretic methods, they all obey a uniform distribution on Ω . Therefore, the sampling methods in this section are all sampling under a uniform distribution. And without loss of generality, in all subsequent derivations, we choose $\alpha_1 = \alpha_2 = 1$.

Assumption 1. (Lipschitz continuity) For any bounded neural network parameters θ_1 and θ_2 , there exists a postive constant **L** such that the empirical loss function satisfies

$$\|\nabla \mathcal{L}_N(\mathbf{x}; \theta_1) - \nabla \mathcal{L}_N(\mathbf{x}; \theta_2)\|_2 \le \mathbf{L}\|\theta_1 - \theta_2\|_2. \tag{10}$$

Assumption 1 is a common assumption in optimization analysis because it can be used to derive an important formula, also known as descent lemma Eq 11.

$$\mathcal{L}_{N}(\boldsymbol{x}; \boldsymbol{\theta}_{1}) \leq \mathcal{L}_{N}(\boldsymbol{x}; \boldsymbol{\theta}_{2}) + \nabla \mathcal{L}_{N}(\boldsymbol{x}; \boldsymbol{\theta}_{2})^{T} (\boldsymbol{\theta}_{1} - \boldsymbol{\theta}_{2}) + \frac{1}{2} \mathbf{L} \|\boldsymbol{\theta}_{1} - \boldsymbol{\theta}_{2}\|_{2}^{2}.$$

$$(11)$$

Assumption 2. For any bounded neural network parameters θ_1 and θ_2 , there exists a constant c such that the empirical loss function satisfies

$$\mathcal{L}_{N}(\boldsymbol{x}; \boldsymbol{\theta}_{1}) \geq \mathcal{L}_{N}(\boldsymbol{x}; \boldsymbol{\theta}_{2}) + \nabla \mathcal{L}_{N}(\boldsymbol{x}; \boldsymbol{\theta}_{2})^{T} (\boldsymbol{\theta}_{1} - \boldsymbol{\theta}_{2}) + \frac{c}{2} \|\boldsymbol{\theta}_{1} - \boldsymbol{\theta}_{2}\|_{2}^{2}. \tag{12}$$

Assumption 2 states that the empirical loss function is strongly convex with respect to θ . Actually, the empirical loss function of neural networks is not always strongly convex, such as when using deep hidden layers and some nonlinear activation functions. However, the strong convexity shown in assumption 2 is necessary to obtain Eq 13. Under assumption 2, if θ^* is the unique global minimizer, according to [1], for any bounded parameter θ , we have

$$2c(\mathcal{L}_N(\mathbf{x};\theta) - \mathcal{L}_N(\mathbf{x};\theta^*)) \le \|\mathcal{L}_N(\mathbf{x};\theta)\|_2^2, \ c \le \mathbf{L}. \tag{13}$$

Recall Algorithm 1, the parameter update equation at the i+1st iteration in the stochastic gradient descent method is shown as follows,

$$\theta_{i+1} = \theta_i - \eta_i g(x_i, \theta_i),$$

where η_i is the step size at the i+1st iteration. Following [2], we give the following assumption about the stochastic gradient vector $g(x_i, \theta_i) = \frac{\partial \mathcal{L}_N((x_i; \theta_i))}{\partial \theta_i}$.

Assumption 3. For the stochastic gradient vector $g(x_i, \theta_i) := \frac{\partial \mathcal{L}_N((x_i; \theta_i))}{\partial \theta_i}$, $\forall i \in \mathbb{N}^+$,

(i) There exists $0 < \mu \le \mu_G$ such that the expectation $\mathbb{E}_{x_i}\left(g(x_i, \theta_i)\right)$ satisfies,

$$\nabla \mathcal{L}_{N}(\boldsymbol{x}; \boldsymbol{\theta}_{i})^{T} \mathbb{E}_{\boldsymbol{x}_{i}} \left(g(\boldsymbol{x}_{i}, \boldsymbol{\theta}_{i}) \right) \ge \mu (1 + r(N_{r}, N_{b})) \|\nabla \mathcal{L}_{N}(\boldsymbol{x}; \boldsymbol{\theta}_{i})\|_{2}^{2}, \tag{14}$$

$$\|\mathbb{E}_{x_i} \left(g(x_i, \theta_i) \right) \|_2 \le \mu_G (1 + r(N_r, N_b)) \|\nabla \mathcal{L}_N(\mathbf{x}; \theta_i)\|_2. \tag{15}$$

(ii) There exist $C_V \ge 0$ and $M_V \ge 0$ such that the variance $\mathbb{V}_{x_i}\left(g(x_i, \theta_i)\right)$ satisfies,

$$V_{x_i}(g(x_i, \theta_i)) \le C_V r(N_r, N_b) + M_V (1 + r(N_r, N_b)) \|\nabla \mathcal{L}_N(\mathbf{x}; \theta_i)\|_2^2, \tag{16}$$

In assumption 3, $r(N_r, N_b)$ is the square of the error between the empirical loss function \mathcal{L}_N and the loss function in integral form \mathcal{L} . For example, if the conditions of Lemma 1 are satisfied, then $r(N_r, N_b) = \left(\boldsymbol{O}\left(N_r^{-\frac{1}{2}}\right) + \boldsymbol{O}\left(N_d^{-\frac{1}{2}}\right)\right)^2$ for the uniform random sapling and $r(N_r, N_b) = \left(\boldsymbol{O}\left(\frac{(\log N_r)^d}{N_r}\right) + \boldsymbol{O}\left(N_d^{-\frac{1}{2}}\right)\right)^2$ for the GLP set.

Theorem 1. Suppose that the stepsize η is fixed and it satisfies

$$0 < \eta \le \frac{\mu}{\mathbf{L} \left(M_V + \mu_G^2 (1 + r(N_r, N_b)) \right)}.$$

Under assumptions (1,2,3), we have

$$\lim_{i \to \infty} \mathbb{E}\left(\mathcal{L}_N(\mathbf{x}; \theta_i)\right) = \frac{\eta \mathbf{L} C_V}{2c\mu} r(N_r, N_b) \tag{17}$$

Proof. Under Eq 11, we have,

$$\mathcal{L}_N(\mathbf{x}; \theta_{i+1}) \le \mathcal{L}_N(\mathbf{x}; \theta_i) + \nabla \mathcal{L}_N(\mathbf{x}; \theta_i)^T (\theta_{i+1} - \theta_i) + \frac{1}{2} \mathbf{L} \|\theta_{i+1} - \theta_i\|_2^2.$$
(18)

According to the stochastic gradient descent method,

$$\theta_{i+1} = \theta_i - \eta g(x_i, \theta_i). \tag{19}$$

Substitute Eq 19 into Eq 18 and find the expectation for x,

$$\mathbb{E}_{x_i} \left(\mathcal{L}_N(\mathbf{x}; \theta_{i+1}) \right) \le \mathcal{L}_N(\mathbf{x}; \theta_i) - \eta \nabla \mathcal{L}_N(\mathbf{x}; \theta_i)^T \mathbb{E}_{x_i} \left(g(x_i; \theta_i) \right) + \frac{\eta^2}{2} \mathbf{L} \mathbb{E}_{x_i} \left(\| g(x_i, \theta_i) \|_2^2 \right). \tag{20}$$

According to Eq (15 and 16) in assumption 3,

$$\mathbb{E}_{x_{i}}\left(\|g(x_{i},\theta_{i})\|_{2}^{2}\right) = \mathbb{V}_{x_{i}}\left(g(x_{i},\theta_{i})\right) + \|\mathbb{E}_{x_{i}}\left(g(x_{i},\theta_{i})\right)\|_{2}^{2} \\ \leq C_{V}r(N_{r},N_{b}) + \left(M_{V} + \mu_{G}^{2}(1 + r(N_{r},N_{b}))\right)(1 + r(N_{r},N_{b}))\|\nabla\mathcal{L}_{N}(\mathbf{x};\theta_{i})\|_{2}^{2}$$
(21)

Using Eq (14 and 21), we can write Eq 20 in the following form,

$$\mathbb{E}_{x_{i}}\left(\mathcal{L}_{N}(\boldsymbol{x};\theta_{i+1})\right) - \mathcal{L}_{N}(\boldsymbol{x};\theta_{i}) \leq \frac{\eta^{2}}{2} \mathbf{L} \mathbb{E}_{x_{i}}\left(\|g(x_{i},\theta_{i})\|_{2}^{2}\right) - \eta \nabla \mathcal{L}_{N}(\boldsymbol{x};\theta_{i})^{T} \mathbb{E}_{x_{i}}\left(g(x_{i};\theta_{i})\right) \\
\leq \frac{\eta^{2}}{2} \mathbf{L} C_{V} r(N_{r},N_{b}) + \frac{\eta^{2}}{2} \mathbf{L}\left(M_{V} + \mu_{G}^{2}(1 + r(N_{r},N_{b}))\right) (1 + r(N_{r},N_{b})) \|\nabla \mathcal{L}_{N}(\boldsymbol{x};\theta_{i})\|_{2}^{2} \\
- \eta \mu (1 + r(N_{r},N_{b})) \|\nabla \mathcal{L}_{N}(\boldsymbol{x};\theta_{i})\|_{2}^{2} \\
= \frac{\eta^{2}}{2} \mathbf{L} C_{V} r(N_{r},N_{b}) - (\eta \mu - \frac{\eta^{2}}{2} \mathbf{L}\left(M_{V} + \mu_{G}^{2}(1 + r(N_{r},N_{b}))\right) (1 + r(N_{r},N_{b})) \|\nabla \mathcal{L}_{N}(\boldsymbol{x};\theta_{i})\|_{2}^{2}.$$
(22)

Since η is fixed and it satisfies

$$0 < \eta \le \frac{\mu}{\mathbf{L} \left(M_V + \mu_G^2 (1 + r(N_r, N_b)) \right)} \tag{23}$$

Then, we have

$$\begin{split} \mathbb{E}_{x_{i}}\left(\mathcal{L}_{N}(\boldsymbol{x};\boldsymbol{\theta}_{i+1})\right) - \mathcal{L}_{N}(\boldsymbol{x};\boldsymbol{\theta}_{i}) \\ &\leq \frac{\eta^{2}}{2}\mathbf{L}C_{V}r(N_{r},N_{b}) - (\eta\mu - \frac{\eta^{2}}{2}\mathbf{L}\left(M_{V} + \mu_{G}^{2}(1 + r(N_{r},N_{b}))\right))(1 + r(N_{r},N_{b}))\|\nabla\mathcal{L}_{N}(\boldsymbol{x};\boldsymbol{\theta}_{i})\|_{2}^{2} \\ &\leq \frac{\eta^{2}}{2}\mathbf{L}C_{V}r(N_{r},N_{b}) - \frac{\mu\eta}{2}(1 + r(N_{r},N_{b}))\|\nabla\mathcal{L}_{N}(\boldsymbol{x};\boldsymbol{\theta}_{i})\|_{2}^{2} \end{split} \tag{24}$$

By Eq 13,

$$\mathbb{E}_{x_{i}}\left(\mathcal{L}_{N}(\boldsymbol{x};\boldsymbol{\theta}_{i+1})\right) - \mathcal{L}_{N}(\boldsymbol{x};\boldsymbol{\theta}_{i}) \leq \frac{\eta^{2}}{2} \mathbf{L} C_{V} r(N_{r},N_{b}) - \frac{\mu \eta}{2} (1 + r(N_{r},N_{b})) \|\nabla \mathcal{L}_{N}(\boldsymbol{x};\boldsymbol{\theta}_{i})\|_{2}^{2} \\
\leq \frac{\eta^{2}}{2} \mathbf{L} C_{V} r(N_{r},N_{b}) - c \mu \eta (1 + r(N_{r},N_{b})) \left(\mathcal{L}_{N}(\boldsymbol{x};\boldsymbol{\theta}_{i}) - \mathcal{L}_{N}(\boldsymbol{x};\boldsymbol{\theta}^{*})\right) \\
\leq \frac{\eta^{2}}{2} \mathbf{L} C_{V} r(N_{r},N_{b}) - c \mu \eta \left(\mathcal{L}_{N}(\boldsymbol{x};\boldsymbol{\theta}_{i}) - \mathcal{L}_{N}(\boldsymbol{x};\boldsymbol{\theta}^{*})\right) \tag{25}$$

Since $\mathcal{L}_N(\mathbf{x}; \theta^*) = 0$, adding $\mathcal{L}_N(\mathbf{x}; \theta_i)$ to both sides of Eq 24 and taking total expectation yields

$$\mathbb{E}\left(\mathcal{L}_{N}(\boldsymbol{x};\boldsymbol{\theta}_{i+1})\right) \leq (1 - c\mu\eta)\mathbb{E}\left(\mathcal{L}_{N}(\boldsymbol{x};\boldsymbol{\theta}_{i})\right) + \frac{\eta^{2}}{2}\mathbf{L}C_{V}r(N_{r},N_{b}) \tag{26}$$

Then we have,

$$\mathbb{E}\left(\mathcal{L}_{N}(\boldsymbol{x};\theta_{i+1})\right) - \frac{\eta \mathbf{L}C_{V}}{2c\mu}r(N_{r},N_{b}) \leq (1 - c\mu\eta)\left(\mathbb{E}\left(\mathcal{L}_{N}(\boldsymbol{x};\theta_{i})\right) - \frac{\eta \mathbf{L}C_{V}}{2c\mu}r(N_{r},N_{b})\right) \\
\leq (1 - c\mu\eta)^{2}\left(\mathbb{E}\left(\mathcal{L}_{N}(\boldsymbol{x};\theta_{i-1})\right) - \frac{\eta \mathbf{L}C_{V}}{2c\mu}r(N_{r},N_{b})\right) \\
\leq (1 - c\mu\eta)^{i}\left(\mathbb{E}\left(\mathcal{L}_{N}(\boldsymbol{x};\theta_{i-1})\right) - \frac{\eta \mathbf{L}C_{V}}{2c\mu}r(N_{r},N_{b})\right)$$
(27)

Since $0 < c\mu\eta \le \frac{c\mu^2}{\mathbf{L}\left(M_V + \mu_G^2(1 + r(N_r, N_b))\right)} \le \frac{c\mu^2}{\mathbf{L}\mu^2} \le 1$, then we have the following conclusion,

$$\lim_{i \to \infty} \mathbb{E}\left(\mathcal{L}_N(\mathbf{x}; \theta_i)\right) = \frac{\eta \mathbf{L}C_V}{2c\mu} r(N_r, N_b) \tag{28}$$

Similar as [25] and [29], the following stability bound assumption is given.

Assumption 4. Let $\mathbb{L}_2(\Omega)$ be the L2 space defined on Ω , the following assumption holds

$$C_1 \|\mathbf{u}\|_2 \le \|\mathcal{A}(\mathbf{u})\|_2 + \|\mathcal{B}(\mathbf{u})\|_2 \le C_2 \|\mathbf{u}\|_2, \ \forall \mathbf{u} \in \mathbb{L}_2(\Omega), \tag{29}$$

where A and B in Eq (1) are linear operators, C_1 and C_2 are positive constants.

Theorem 2. Suppose Assumption 4 hold, let $\mathbf{u}^* \in \mathbb{L}_2(\Omega)$ be the exact solution of Eq (1). If $r(\mathbf{x}; \theta) \in \Omega = [0, 1]^d$ and $b(\mathbf{x}; \theta) \in \Omega = [0, 1]^d$ have continuous partial derivatives, then the following error estimate holds (i)when $\{\mathbf{x}_i\}_{i=1}^{N_r}$ is a good lattice points set,

$$\|\boldsymbol{u}^{*}(\boldsymbol{x}) - \boldsymbol{u}(\boldsymbol{x}; \boldsymbol{\theta})\|_{2} \leq \frac{\sqrt{2}}{C_{1}} \left(\mathcal{L}_{r, N_{r}}^{GLP} + \mathcal{L}_{b, N_{b}}^{UR} + O\left(\frac{(\log N_{r})^{d}}{N_{r}}\right) + O\left(N_{b}^{-\frac{1}{2}}\right) \right)^{\frac{1}{2}}, \tag{30}$$

(ii)when $\{x_i\}_{i=1}^{N_r}$ is a uniform random sampling points set,

$$\|\boldsymbol{u}^{*}(\boldsymbol{x}) - \boldsymbol{u}(\boldsymbol{x}; \boldsymbol{\theta})\|_{2} \leq \frac{\sqrt{2}}{C_{1}} \left(\mathcal{L}_{r, N_{r}}^{UR} + \mathcal{L}_{b, N_{b}}^{UR} + \boldsymbol{O}\left(N_{r}^{-\frac{1}{2}}\right) + \boldsymbol{O}\left(N_{b}^{-\frac{1}{2}}\right) \right)^{\frac{1}{2}}, \tag{31}$$

Proof. By Assumption 4, we have

$$C_{1}\|\mathbf{u}^{*}(\mathbf{x}) - \mathbf{u}(\mathbf{x};\theta)\|_{2} \leq \|\mathcal{A}(\mathbf{u}^{*}(\mathbf{x})) - \mathcal{A}(\mathbf{u}(\mathbf{x};\theta))\|_{2} + \|\mathcal{B}(\mathbf{u}^{*}(\mathbf{x})) - \mathcal{B}(\mathbf{u}(\mathbf{x};\theta))\|_{2}$$

$$= \|\mathcal{A}(\mathbf{u}(\mathbf{x};\theta)) - f(\mathbf{x})\|_{2} + \|\mathcal{B}(\mathbf{u}(\mathbf{x};\theta)) - g(\mathbf{x})\|_{2}$$

$$= \|r(\mathbf{x};\theta)\|_{2} + \|b(\mathbf{x};\theta)\|_{2}$$

$$\leq \sqrt{2} \left(\|r(\mathbf{x};\theta)\|_{2}^{2} + \|b(\mathbf{x};\theta)\|_{2}^{2} \right)^{\frac{1}{2}}.$$
(32)

Since $r(x; \theta) \in \Omega = [0, 1]^d$ and $b(x; \theta) \in \Omega = [0, 1]^d$ have continuous partial derivatives, then using Lemma 1, we have

$$\mathcal{L}_{r}(\boldsymbol{x};\theta) = \|r(\boldsymbol{x};\theta)\|_{2}^{2} \leq \mathcal{L}_{r,N_{r}}^{GLP}(\boldsymbol{x};\theta) + \boldsymbol{O}\left(\frac{(\log N_{r})^{d}}{N_{r}}\right),$$

$$\mathcal{L}_{b}(\boldsymbol{x};\theta) = \|b(\boldsymbol{x};\theta)\|_{2}^{2} \leq \mathcal{L}_{b,N_{b}}^{UR}(\boldsymbol{x};\theta) + \boldsymbol{O}\left(N_{b}^{-\frac{1}{2}}\right)$$
(33)

Therefore,

$$\|\boldsymbol{u}^{*}(\boldsymbol{x}) - \boldsymbol{u}(\boldsymbol{x}; \theta)\|_{2} \leq \frac{\sqrt{2}}{C_{1}} (\|r(\boldsymbol{x}; \theta)\|_{2}^{2} + \|b(\boldsymbol{x}; \theta)\|_{2}^{2})^{\frac{1}{2}}$$

$$\leq \frac{\sqrt{2}}{C_{1}} \left(\mathcal{L}_{r, N_{r}}^{GLP} + \mathcal{L}_{b, N_{b}}^{UR} + \boldsymbol{O}\left(\frac{(\log N_{r})^{d}}{N_{r}}\right) + \boldsymbol{O}\left(N_{b}^{-\frac{1}{2}}\right) \right)^{\frac{1}{2}}.$$
(34)

Similar steps can be taken to prove Eq 31, which is omitted here.

Corollary 1. Suppose that Theorem 1 and Theorem 2 hold, then we have (i) If $\{x_k\}_{k=1}^{N_r}$ is a good lattice points set,

$$\lim_{i \to \infty} \mathbb{E}\left(\|\boldsymbol{u}^{*}(\boldsymbol{x}) - \boldsymbol{u}(\boldsymbol{x}; \theta_{i})\|_{2}^{2}\right) \leq \frac{2}{C_{1}^{2}} \left(\frac{\eta L C_{V}}{2c\mu} \left(\boldsymbol{O}\left(\frac{(\log N_{r})^{d}}{N_{r}}\right) + \boldsymbol{O}\left(N_{b}^{-\frac{1}{2}}\right)\right)^{2} + \boldsymbol{O}\left(\frac{(\log N_{r})^{d}}{N_{r}}\right) + \boldsymbol{O}\left(N_{b}^{-\frac{1}{2}}\right)\right). \tag{35}$$

(ii) If $\{x_k\}_{k=1}^{N_r}$ is a uniform random sampling points set,

$$\lim_{i \to \infty} \mathbb{E}\left(\|\boldsymbol{u}^{*}(\boldsymbol{x}) - \boldsymbol{u}(\boldsymbol{x}; \boldsymbol{\theta}_{i})\|_{2}^{2}\right) \leq \frac{2}{C_{1}^{2}} \left(\frac{\eta \mathbf{L} C_{V}}{2c\mu} \left(\boldsymbol{O}\left(N_{r}^{-\frac{1}{2}}\right) + \boldsymbol{O}\left(N_{b}^{-\frac{1}{2}}\right)\right)^{2} + \boldsymbol{O}\left(N_{r}^{-\frac{1}{2}}\right) + \boldsymbol{O}\left(N_{b}^{-\frac{1}{2}}\right)\right). \tag{36}$$

Proof. By Theorem 1,

$$\lim_{i \to \infty} \mathbb{E}\left(\mathcal{L}_N(\mathbf{x}; \theta_i)\right) = \frac{\eta \mathbf{L}C_V}{2c\mu} r(N_r, N_b) \tag{37}$$

Thus, if $\{x_i\}_{i=1}^{N_r}$ is a good lattice points set,

$$\lim_{i \to \infty} \mathbb{E}\left(\mathcal{L}_{r,N_r}^{GLP}(\mathbf{x}; \theta_i) + \mathcal{L}_{b,N_b}^{UR}(\mathbf{x}; \theta_i)\right) = \frac{\eta \mathbf{L} C_V}{2c\mu} \left(\mathbf{O}\left(\frac{(\log N_r)^d}{N_r}\right) + \mathbf{O}\left(N_b^{-\frac{1}{2}}\right)\right)^2$$
(38)

By Theorem 2,

$$\|\boldsymbol{u}^{*}(\boldsymbol{x}) - \boldsymbol{u}(\boldsymbol{x}; \boldsymbol{\theta})\|_{2} \leq \frac{\sqrt{2}}{C_{1}} \left(\mathcal{L}_{r, N_{r}}^{GLP} + \mathcal{L}_{b, N_{b}}^{UR} + \boldsymbol{O}\left(\frac{(\log N_{r})^{d}}{N_{r}}\right) + \boldsymbol{O}\left(N_{b}^{-\frac{1}{2}}\right) \right)^{\frac{1}{2}}. \tag{39}$$

Squaring both sides of the inequality and taking the expectation yields

$$\mathbb{E}\left(\|\boldsymbol{u}^*(\boldsymbol{x}) - \boldsymbol{u}(\boldsymbol{x}; \boldsymbol{\theta}_i)\|_2^2\right) \le \frac{2}{C_1^2} \left(\mathbb{E}\left(\mathcal{L}_{r, N_r}^{GLP} + \mathcal{L}_{b, N_b}^{UR}\right) + \boldsymbol{O}\left(\frac{(\log N_r)^d}{N_r}\right) + \boldsymbol{O}\left(N_b^{-\frac{1}{2}}\right)\right). \tag{40}$$

Combining Eq (38 and 40), we have

$$\lim_{i \to \infty} \mathbb{E}\left(\|\boldsymbol{u}^*(\boldsymbol{x}) - \boldsymbol{u}(\boldsymbol{x}; \theta_i)\|_2^2\right) \le \frac{2}{C_1^2} \left(\frac{\eta \mathbf{L} C_V}{2c\mu} \left(\boldsymbol{O}\left(\frac{(\log N_r)^d}{N_r}\right) + \boldsymbol{O}\left(N_b^{-\frac{1}{2}}\right)\right)^2 + \boldsymbol{O}\left(\frac{(\log N_r)^d}{N_r}\right) + \boldsymbol{O}\left(N_b^{-\frac{1}{2}}\right)\right). \tag{41}$$

Similar steps can be taken to prove Eq 36, which is omitted here.

Remark 2. It is a well known fact that $O\left(\frac{(\log N_r)^d}{N_r}\right) < O\left(N_r^{-\frac{1}{2}}\right)$ when N_r is large. That is, in Corollary 1, the upper bound on $\lim_{i\to\infty}\mathbb{E}\left(\|\boldsymbol{u}^*(\boldsymbol{x})-\boldsymbol{u}(\boldsymbol{x};\theta_i)\|_2^2\right)$ is smaller if $\left\{\boldsymbol{x}_i\right\}_{i=1}^{N_r}$ is a good lattice points set when N_r is large. From this point of view, it also shows the effectiveness of the good lattice points set.

 Table 1

 Default settings for main parameters in PINN.

Torch	Activation	Initialization	Optimization	Learning	Loss Weights	Random
Version	Function	Method		Rate	(α_1 / α_2)	Seed
2.4.0	Tanh	Xavier	Adam/LBFGS	0.0001/1	1/1	100

4. Numerical Experiments

4.1. Symbols and parameter settings

The analytical solution is denoted by u^* ; u^{UR} and u^{GLP} are used to denote the approximate solutions under uniform random sampling and good lattice points set, respectively. The relative errors in the test set $\{x_i\}_{i=1}^{M_t}$ sampled from the uniform random sampling method are defined as follows

$$e_{\infty}(u^{\mathrm{UR}}) = \frac{\|u^* - u^{\mathrm{UR}}\|_{\infty}}{\|u^*\|_{\infty}} = \frac{\max\limits_{1 \le i \le M_t} |u^*(x_i) - u^{\mathrm{UR}}(x_i; \theta)|}{\max\limits_{1 \le i \le M_t} |u^*(x_i)|},$$

$$e_2(u^{\mathrm{UR}}) = \frac{\|u^* - u^{\mathrm{UR}}\|_2}{\|u^*\|_2} = \frac{\sum_{i=1}^{M_t} \sqrt{|u^*(x_i) - u^{\mathrm{UR}}(x_i; \theta)|^2}}{\sum_{i=1}^{M_t} \sqrt{|u^*(x_i)|^2}}.$$
(42)

When calculating the relative errors Eq 42 in the code, we call the **numpy.linalg.norm** function; and when doing random uniform sampling, we call the **numpy.random** function. In order to reduce the effect of randomness on the calculation results, this paper sets all the seeds of the random numbers to 100. The default parameter settings in PINN are given in Table 1. All numerical simulations are carried on NVIDIA A100 with 80GB of memory.

4.2. Two-dimensional Poisson equation

4.2.1. Two-dimensional Poisson equation with one peak

For the following Poisson equation in two-dimensional

$$\begin{cases} -\Delta u(x, y) = f(x, y), & (x, y) \text{ in } \Omega, \\ u(x, y) = g(x, y), & (x, y) \text{ on } \partial\Omega, \end{cases}$$

$$(43)$$

where $\Omega = (-1, 1)^2$, the analytical solution which has a peak at (0, 0) is chosen as (see Fig 1(a))

$$u = e^{-1000(x^2 + y^2)}. (44)$$

The Dirichlet boundary condition g(x, y) and the source function f(x, y) are given by Eq 44.

In order to compare our method with other five methods, we sample 10946 points in Ω and 1000 points on $\partial\Omega$ as the training set and 400×400 points as the test set for all the methods. In the following experiments, PINNs were all trained 50000 epochs. More detailed parameters can be found in Table 1. Six different uniform sampling methods are implemented: (1) uniform random sampling; (2) LHS method; (3) Halton sequence; (4) Hammersley sequence; (5) Sobol sequence; (6) GLP set. In code, methods (2)–(5) are implemented by the DeepXDE package [13].

The numerical results of uniform random sampling are given in Fig 2, Fig 2(a) is the analytical solution, Fig 2(b) is training points sampled by uniform random sampling method(Eq.44), Fig 2(c) is the approximate solution of PINN under uniform random sampling, and Fig 2(d) is the absolute error.

Similarly, the numerical results for LHS mehtod, Halton Sequence, Hammersley Sequence, Sobel Sequence and GLP set are given in Fig (3, 4, 5, 6, 7), respectively.

The figure labeled as Fig. 8 illustrates the performance of six distinct methods in terms of their relative errors on the test set throughout the training process. Additionally, Table 2 provides a comparative analysis of the errors obtained using these various methods. Upon examining these results, it is evident that the GLP set yields superior outcomes compared to the other methodologies.

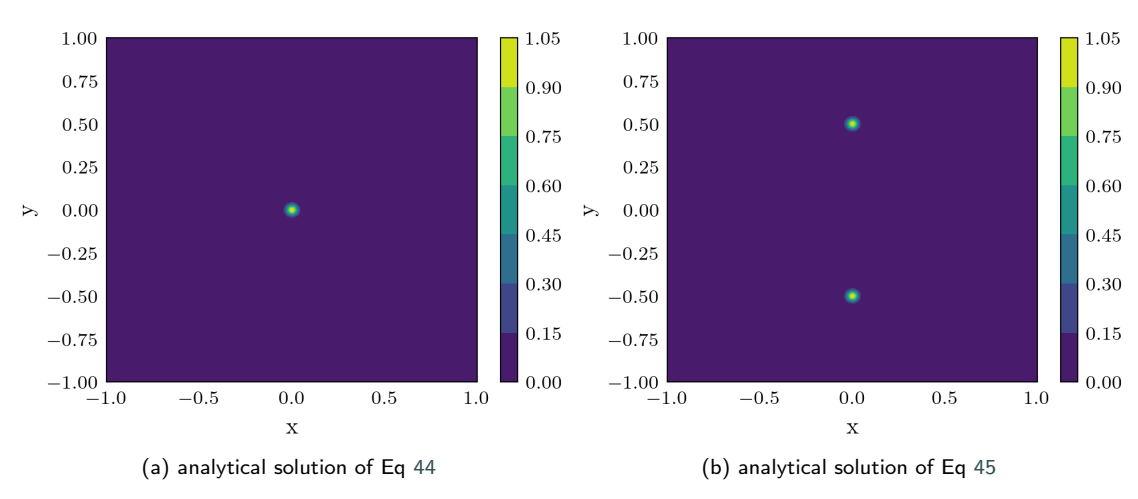


Figure 1: (a) the analytical solution u^* of Eq 44; (b) the analytical solution u^* of Eq 45.

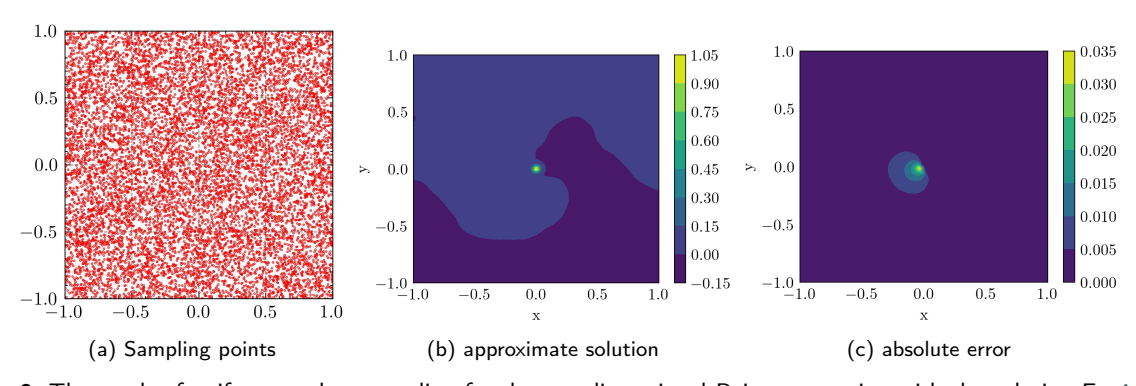


Figure 2: The result of uniform random sampling for the two-dimensional Poisson equation with the solution Eq 44. (a) training points sampled by uniform random sampling method; (b) the approximate solution u^{UR} ; (c) the absolute error $|u^* - u^{UR}|$.

 Table 2

 Comparison of errors under different methods.

Relative	Uniform	LHS	Halton	Hammersley	Sobol	GLP
error	Random	Metohd	Sequence	Sequence	Sequence	set
$e_{\infty}(u)$	3.243×10^{-2}	2.780×10^{-2}	4.963×10^{-2}	1.223×10^{-1}	3.412×10^{-2}	4.475×10^{-3}
<i>e</i> ₂ (<i>u</i>)	1.051×10^{-1}	7.921×10^{-2}	1.858×10^{-1}	3.523×10^{-1}	8.824×10^{-2}	4.045×10^{-2}

4.2.2. Two-dimensional Poisson equation with two peaks

Consider the Poisson equation Eq (43) in previous subsection, the analytical solution which has two peaks is chosen as (see Fig 1(b))

$$u = e^{-1000(x^2 + (y - 0.5)^2)} + e^{-1000(x^2 + (y + 0.5)^2)}.$$
(45)

We sample 10946 points in Ω and 400 points on $\partial\Omega$ as the training set and 400 × 400 points as the test set. The settings of main parameters in PINN are given in Table 1. Similar to the previous subsection, here we still use the GLP set to compare with the other five uniform sampling methods. After 50000 epochs of Adam training and 30000 epochs of LBFGS training, the numerical results based on different sampling methods are shown in Fig (9 and 10). It is worth mentioning that since the residual training points used in this subsection are exactly the same as those used

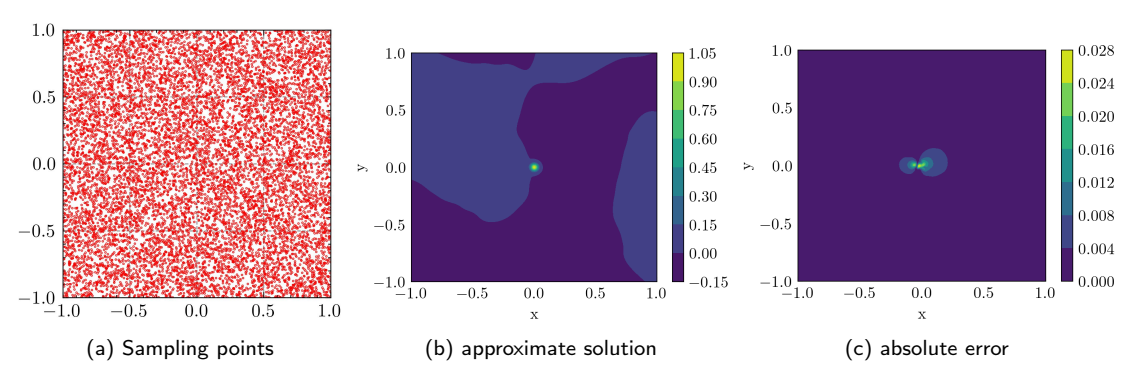


Figure 3: The result of LHS method for the two-dimensional Poisson equation with the solution Eq 44. (a) training points sampled by LHS method; (b) the approximate solution u^{LHS} ; (c) the absolute error $|u^* - u^{\text{LHS}}|$.

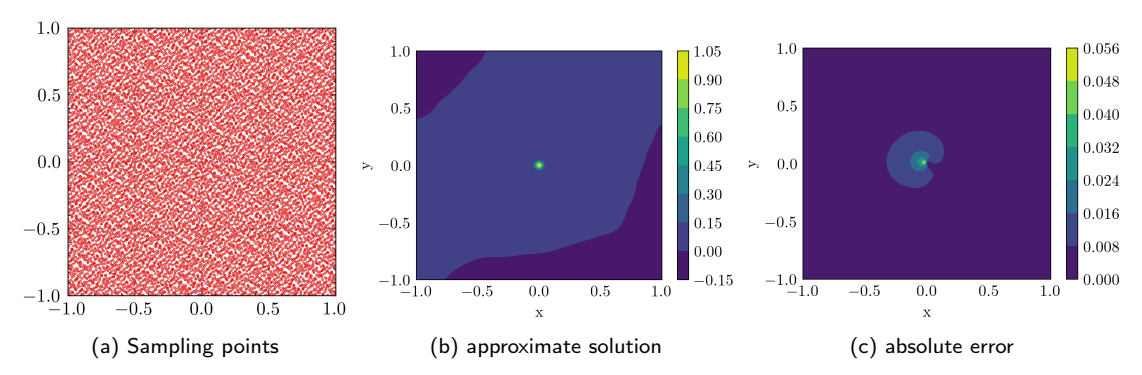


Figure 4: The result of Halton sequence for the two-dimensional Poisson equation with the solution Eq 44. (a) training points sampled by Halton sequence; (b) the approximate solution u^{Halton} ; (c) the absolute error $|u^* - u^{\text{Halton}}|$.

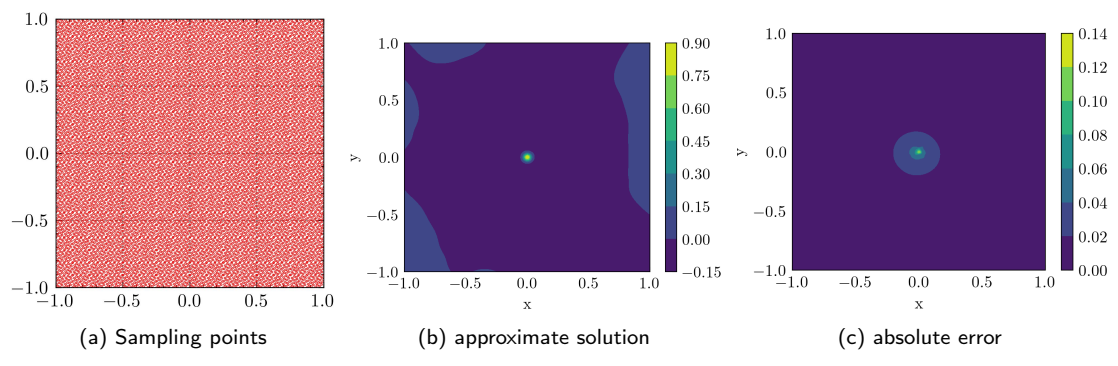


Figure 5: The result of Hammersley sequence for the two-dimensional Poisson equation with the solution Eq 44. (a) training points sampled by Hammersley sequence; (b) the approximate solution $u^{\text{Hammersley}}$; (c) the absolute error $|u^* - u^{\text{Hammersley}}|$.

in the previous subsection, they will not be given repeatedly here and can be seen in Fig (2(a), 3(a), 4(a), 5(a), 6(a)) and (7(a)).

To present the results of these six methods more clearly, we have provided the performance of relative errors during the training process in Fig 11, and the final relative errors of the six methods in Table 3.

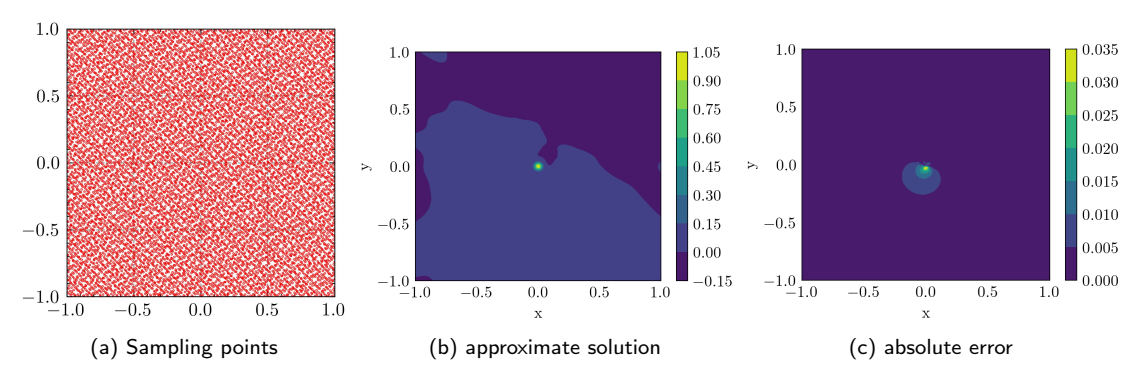


Figure 6: The result of Sobol sequence for the two-dimensional Poisson equation with the solution Eq 44. (a) training points sampled by Sobol sequence; (b) the approximate solution u^{Sobol} ; (c) the absolute error $|u^* - u^{\text{Sobol}}|$.

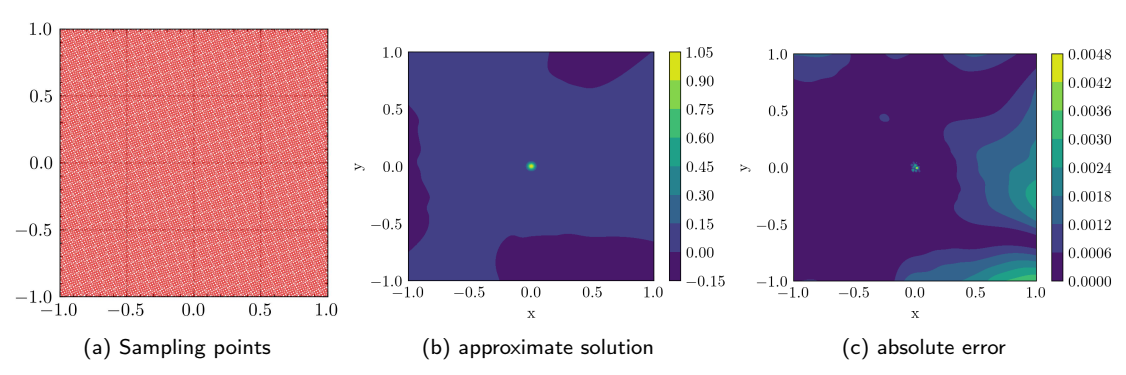


Figure 7: The result of GLP set for the two-dimensional Poisson equation with the solution Eq 44. (a) training points sampled by GLP set; (b) the approximate solution u^{GLP} ; (c) the absolute error $|u^* - u^{\text{GLP}}|$.

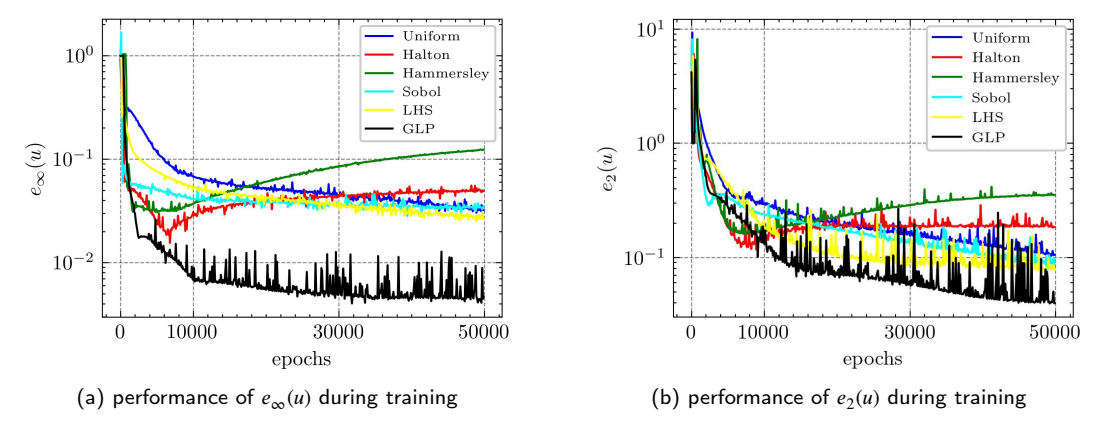


Figure 8: (a) the performance of relative error $e_{\infty}(u)$ with different training epochs, (b) the performance of relative error $e_2(u)$ with different training epochs.

4.3. Inverse problem of two-dimensional Helmholtz equation

For the following two-dimensional Helmholtz equation

$$\begin{cases} \Delta u(x, y) + k^2 u(x, y) = f(x, y), & (x, y) \text{ in } \Omega, \\ u(x, y) = 0, & (x, y) \text{ on } \partial\Omega, \end{cases}$$

$$(46)$$

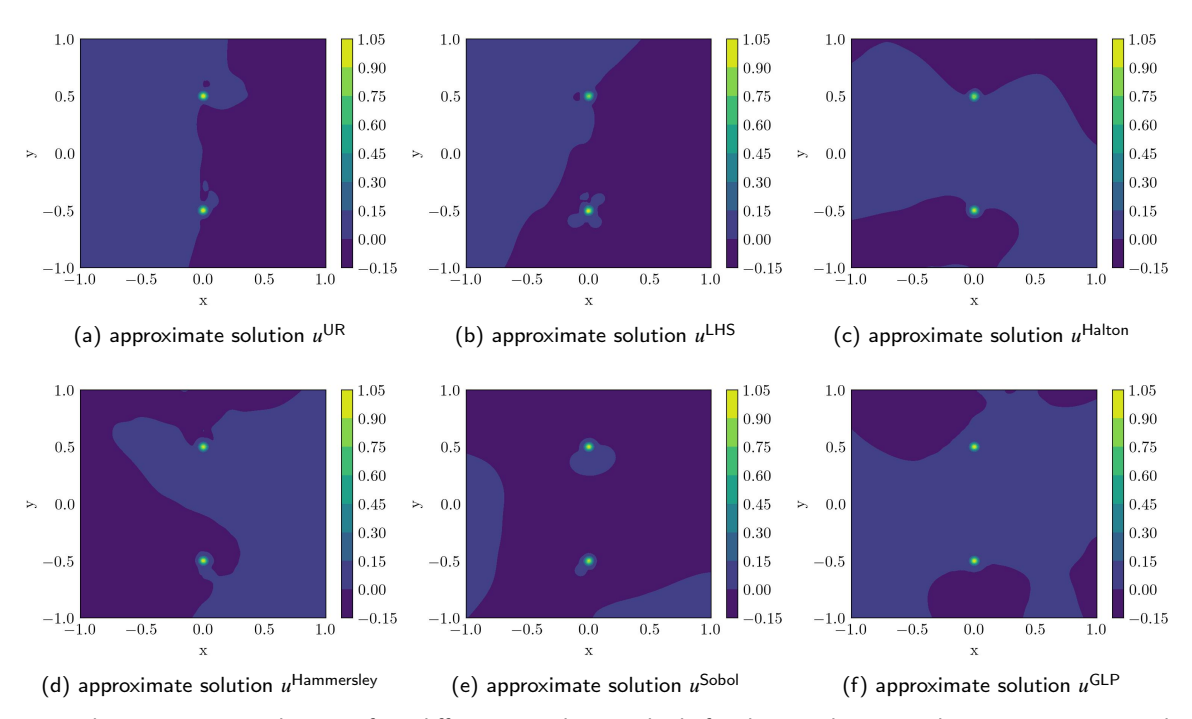


Figure 9: The approximate solutions of six different sampling methods for the two-dimensional Poisson equation with the analytical solution 45.

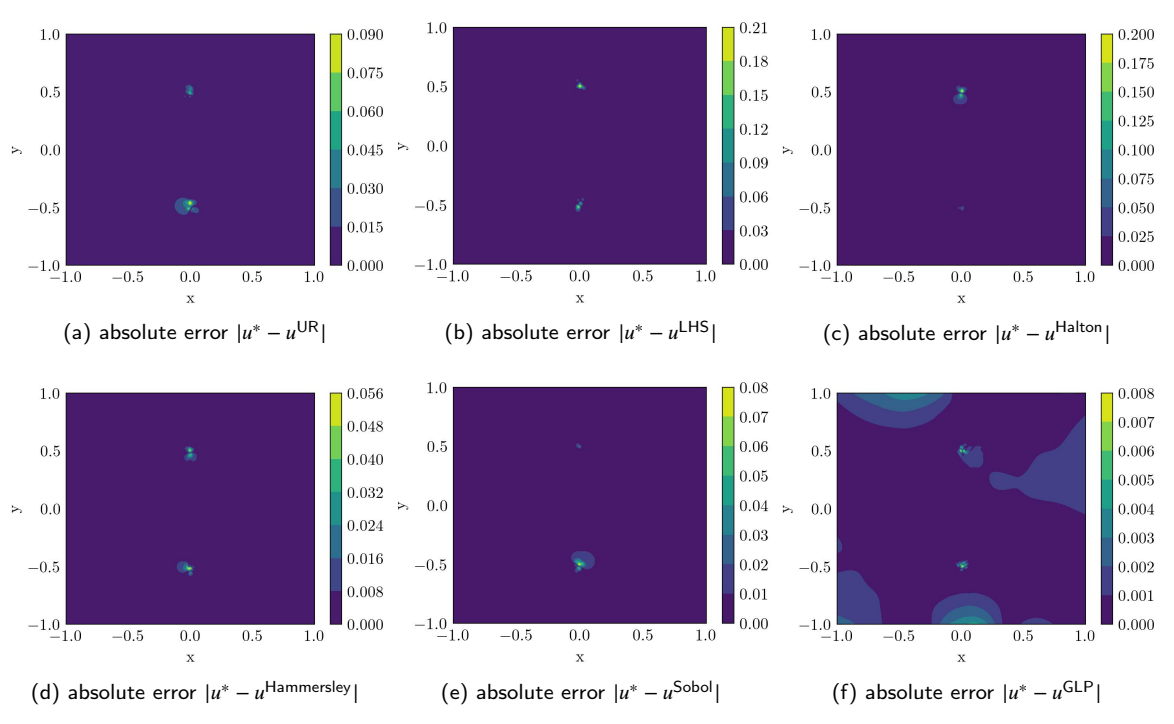


Figure 10: The absolute errors of six different sampling methods for the two-dimensional Poisson equation with the analytical solution 45.

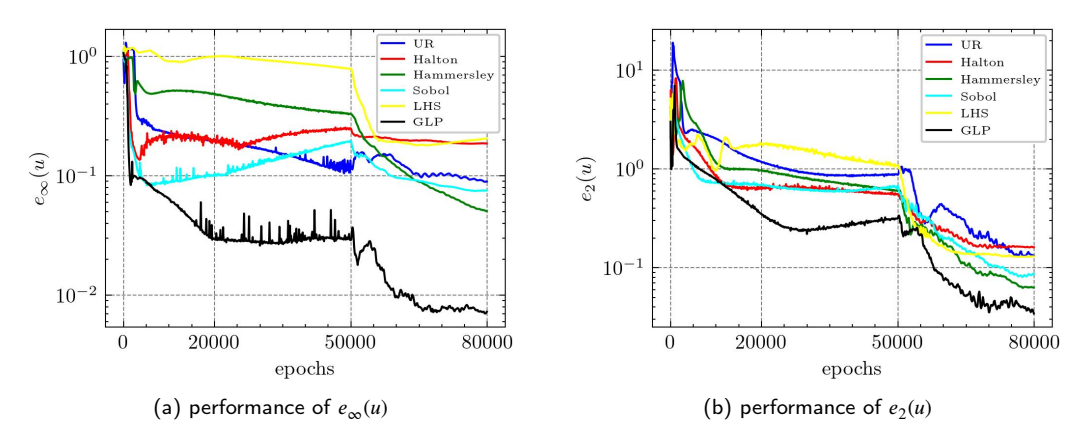


Figure 11: (a) the performance of relative error $e_{\infty}(u)$ with different training epochs; (b) the performance of relative error $e_{2}(u)$ with different training epochs.

 Table 3

 Comparison of errors under different methods.

Ī	Relative error	Uniform Random	LHS Metohd	Halton Sequence	Hammersley Sequence	Sobol Sequence	GLP set
Ì	$e_{\infty}(u)$	8.993×10^{-2}	2.054×10^{-1}	1.866×10^{-1}	5.061×10^{-2}	7.527×10^{-2}	7.406×10^{-3}
ſ	e ₂ (u)	1.332×10^{-1}	1.303×10^{-1}	1.620×10^{-1}	6.304×10^{-2}	8.591×10^{-2}	3.279×10^{-2}

 Table 4

 Comparison of errors between uniform random sampling and GLP set.

Methods \Errors	$e_{\infty}(u)$	$e_2(u)$	$ k^2 - k^{*2} $
UR	1.148×10^{-4}	8.956×10^{-5}	5.871×10^{-1}
GLP	2.273×10^{-5}	1.724×10^{-5}	1.181×10^{-3}

where $\Omega = (0, 1)^2$ and k^2 is the unknown parameter. The analytical solution is given in Eq 47.

$$u = \sin(2\pi x)\sin(2\pi y). \tag{47}$$

We sample 6765 points within Ω as the training set, while utilizing 400×400 points for the test set. Since the Dirichlet boundary conditions here are constant, it is easy for us to use the method of enforcing boundary conditions ([28],[14]) to eliminate the influence of boundary loss. In Fig 12, the details of the GLPset sampling points and the uniform random sampling points are given. The uniformity of the GLP set is clearly better than the uniform random sampling. Furthermore, we extract the analytical solution corresponding to $(k^*)^2 = 9$ for data-driven at 500 points by uniform random sampling. Similar to [18], after adding data-driven training points from the analytic solution, let PINN output not only the approximate solution, but also the parameter k^2 . Here, regarding the initial value of the parameter k^2 , we set k to 0.1. The other settings of main parameters in PINN are given in Table 1.

After completing 50,000 epochs of Adam training and an additional 50,000 epochs of LBFGS training, we compare the numerical results obtained through GLP set with those derived from uniform random sampling to demonstrate the effectiveness of our proposed method.

In Fig 13, the analytic solution, the approximate solution and the absolute error based on uniform random sampling are shown. And the approximate solution and the absolute error based on GLP set are given in Fig 14.

For a clearer comparison between uniform random sampling and GLP set, the performance of the relative errors of the analytical solution u and the absolute error of parameter k^2 during training is given in Fig 15. In order to present the numerical results in more detail, we put the final errors in Table 4. Based on the above numerical results, it is not difficult to see that the GLP set has advantages over uniform random sampling when the number of training points is the same.

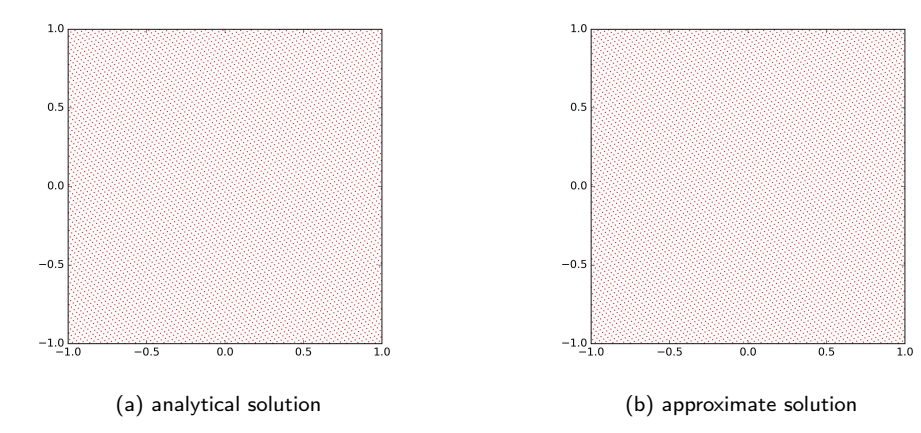


Figure 12: The training points for the inverse problem of two-dimensional Helmholtz equation. (a) the residual training points by uniform random sampling; (b) the residual training points by GLP set.

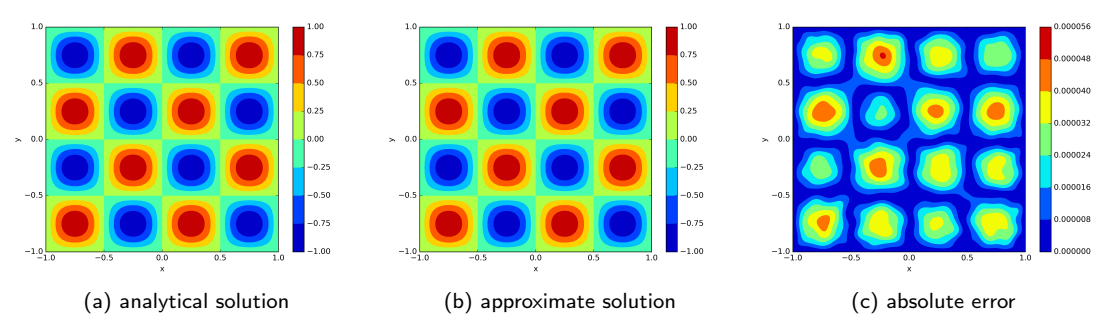


Figure 13: The results of uniform random sampling for the inverse problem of two-dimensional Helmholtz equation. (a) the analytical solution u^* of the equation; (b) the approximate solution u^{UR} ; (d) the absolute error $|u^* - u^{UR}|$.

4.4. High-dimensional Linear Problems

For the following high-dimensional Poisson equation,

$$\begin{cases}
-\Delta u(x) = f(x), & x \text{ in } \Omega, \\
u(x) = g(x), & x \text{ on } \partial\Omega,
\end{cases}$$
(48)

where $\Omega = (0, 1)^d$. The analytical solution is given by Eq 49.

$$u = e^{-p\|\mathbf{x}\|_2^2}. (49)$$

The Dirichlet boundary condition g(x) on $\partial\Omega$ and function f(x) are given by the analytical solution.

4.4.1. Five-dimensional Problems

Here,we take d=5 and p=10 in Eq (48 and 49). And we sample 10007 points in Ω and 100 points in each hyperplane of $\partial\Omega$ as the training set and 200000 points as the test set. In order to verify the statement in Remake 1, we specifically used the Sigmoid activation function for the calculations in this and the next subsection (section 4.4.1 and 4.4.2). The settings of main parameters in PINN are given in Table 1. Since visualizing training points in the high-dimensional case is a challenging task, we only plot the distribution of these 10007 residual training points in the first two dimensions in Fig 16.

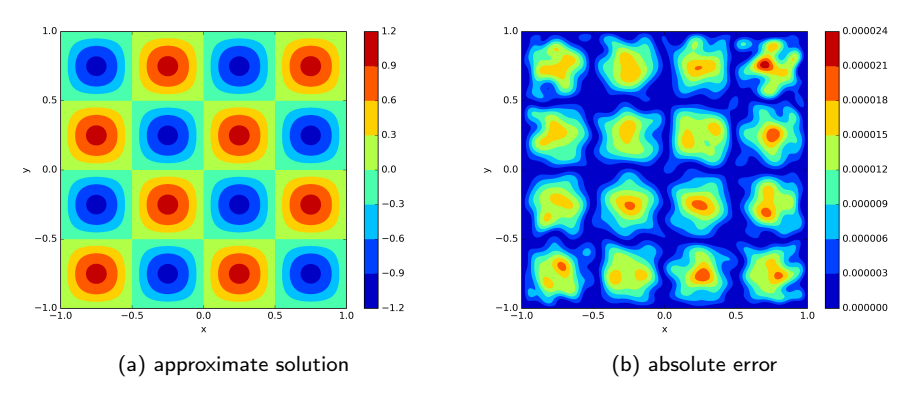


Figure 14: The results of GLP set for the inverse problem of two-dimensional Helmholtz equation. (a) the approximate solution u^{NTM} ; (c) the absolute error $|u^* - u^{NTM}|$.

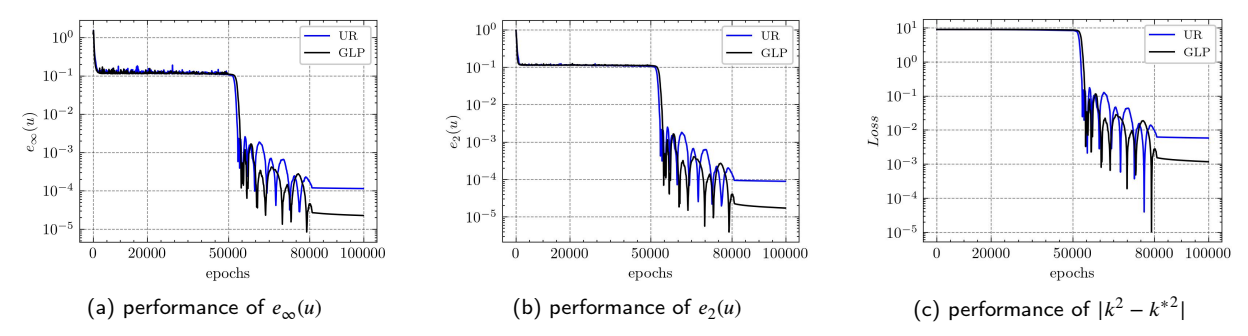


Figure 15: (a) performance of the relative error $e_{\infty}(u)$ with different training epochs; (b) performance of the relative error $e_{1}(u)$ with different training epochs; (c) performance of the absolute error $|k^{*2} - k^{2}|$ with different training epochs.

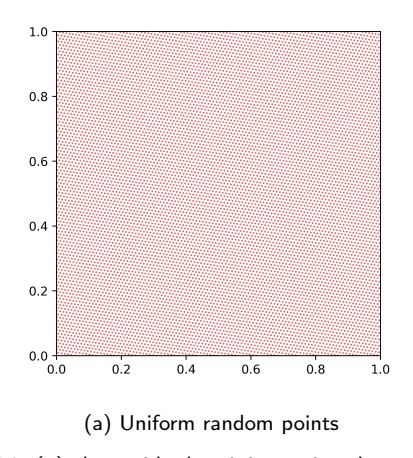
Table 5 The number of residual points in Ω and the number of boundary points at each hyperplane that composes $\partial\Omega$ under sampling strategies.

Strategy	1	2	3	4
Method	UR	UR	UR	GLP
Residual points	10007	33139	51097	10007
Each hyperplane	100	100	100	100
$e_2(u)$	1.890×10^{-3}	1.257×10^{-3}	1.172×10^{-3}	6.950×10^{-4}
$e_{\infty}(u)$	4.755×10^{-4}	4.197×10^{-4}	3.819×10^{-4}	3.182×10^{-4}

In Fig 17, after 50000 epochs of Adam training and 20000 epochs of LBFGS training, we undertake a comparative analysis of the numerical results derived from the GLP set versus those obtained through uniform random sampling. This comparison aims to demonstrate the efficacy of our proposed method for the same number of training points. Furthermore, taking into account the number of training points, we devise various sampling strategies grounded on the quantity of uniform random samples and conduct controlled experiments with the GLP set. The experimental outcomes conclusively demonstrate that the GLP set retains a distinct advantage over uniform random sampling, even when the latter employs approximately five times the number of points. The details and results of the different sampling strategies are summarized in Table 5.

4.4.2. Eight-dimensional Problems

Here, we take d=8 and p=1 in Eq (48 and 49). And we sample 11215 points in Ω and 200 points in each hyperplane of $\partial\Omega$ as the training set and 500000 points as the test set. The settings of main parameters in PINN are



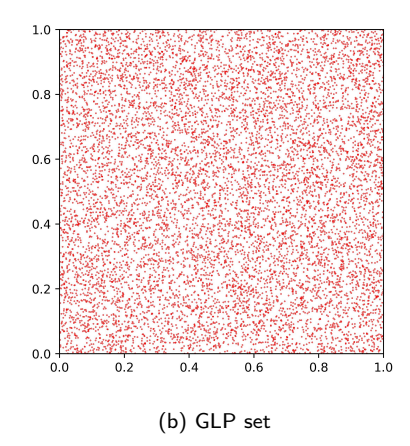


Figure 16: (a) the residual training points by uniform random sampling; (b) the residual training points by GLP set.

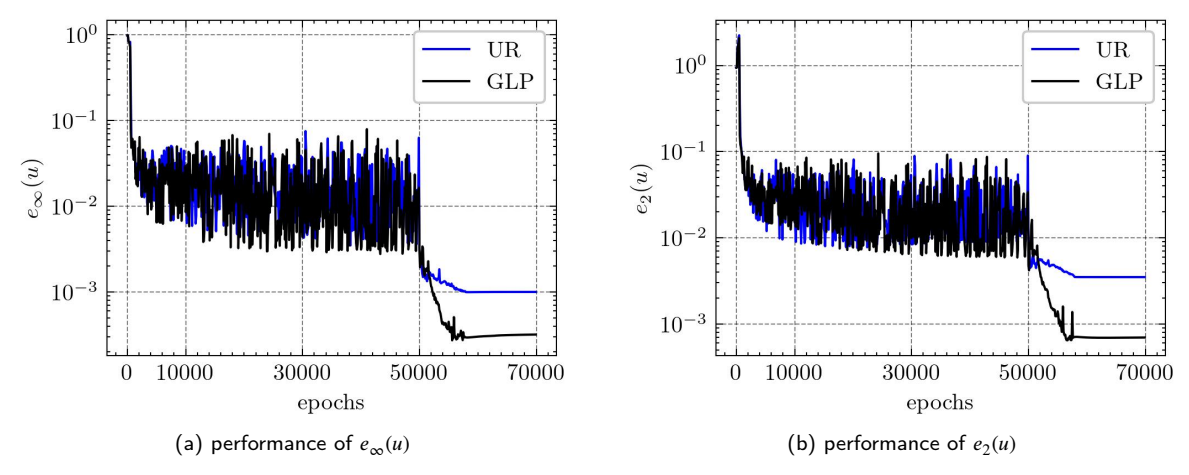


Figure 17: (a) the performance of relative error $e_{\infty}(u)$ during training process; (b) the performance of relative error $e_2(u)$ during training process.

the same as Section 4.4.1. Since visualizing training points in the high-dimensional case is a challenging task, we only plot the distribution of these 11215 residual training points in the first two dimensions in Fig 18.

In Fig 19, after 50000 epochs of Adam training and 20000 epochs of LBFGS training, we undertake a comparative analysis of the numerical results derived from the GLP set versus those obtained through uniform random sampling. This comparison aims to demonstrate the efficacy of our proposed method for the same number of training points. Furthermore, taking into account the number of training points, we devise various sampling strategies grounded on the quantity of uniform random samples and conduct controlled experiments with the GLP set. The experimental results conclusively prove that the GLP set maintains a clear advantage over uniform random sampling. Even though the number of points in uniform random sampling is three times that of the GLP set, the accuracy of the GLP set remains comparable to it. The details and results of the different sampling strategies are summarized in Table 6.

4.5. High-dimensional Nolinear Problems

For the following high-dimensional nolinear equation,

$$\begin{cases}
-\Delta u(x) + u^{3}(x) = f(x), & x \text{ in } \Omega, \\
u(x) = g(x), & x \text{ on } \partial\Omega,
\end{cases}$$
(50)

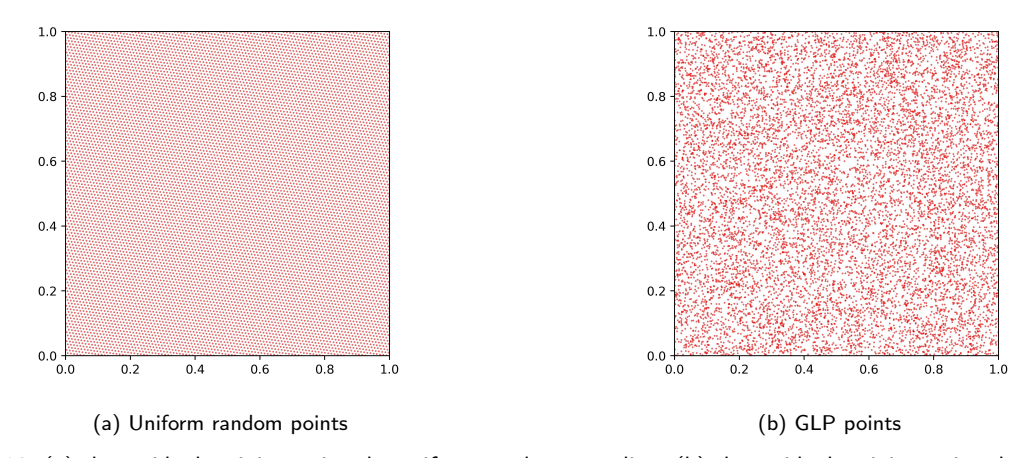


Figure 18: (a) the residual training points by uniform random sampling; (b) the residual training points by GLP set.

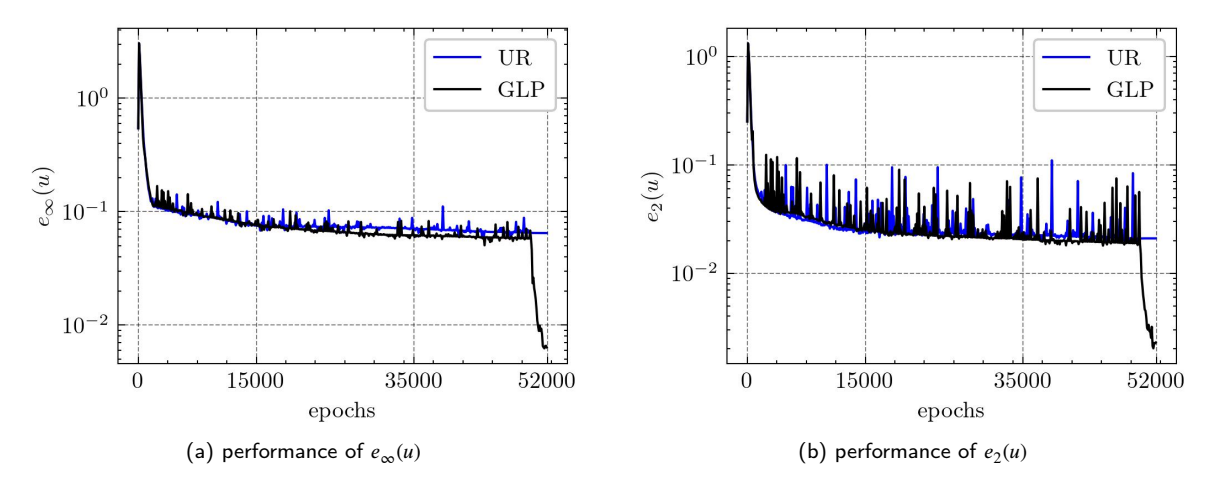


Figure 19: (a) the performance of relative error $e_{\infty}(u)$ during training process; (b) the performance of relative error $e_2(u)$ during training process.

Table 6 The number of residual points in Ω and the number of boundary points at each hyperplane that composes $\partial\Omega$ under sampling strategies.

Strategy	1	2	3	4
Method	UR	UR	UR	GLP
Residual points	11215	24041	33139	11215
Each hyperplane	200	200	200	200
$e_2(u)$	2.096×10^{-2}	1.883×10^{-2}	1.172×10^{-3}	2.287×10^{-3}
$e_{\infty}(u)$	6.481×10^{-2}	5.798×10^{-2}	5.272×10^{-3}	6.3687×10^{-3}

where $\Omega = (0, 1)^d$. The analytical solution is given by Eq 51.

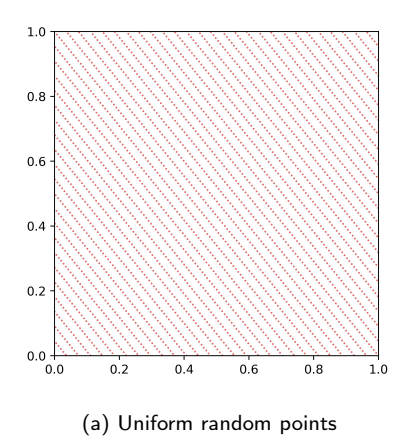
$$u = \sin(\frac{k\pi}{d} \sum_{i=1}^{d} x_i). \tag{51}$$

The source function f(x) and the Dirichlet boundary condition g(x) are given by Eq 51.

4.5.1. Five-dimensional Problems

Here, we take d=5 and k=4 in Eq 51. And we sample 3001 points in Ω and 100 points in each hyperplane of $\partial\Omega$ as the training set and 200000 points as the test set. The settings of main parameters in PINN are given in Table 1.

Visualizing training points in the high-dimensional context poses a significant challenge, hence we restrict our plotting to the distribution of the first two dimensions for these 11215 residual training points, as depicted in Fig 20.



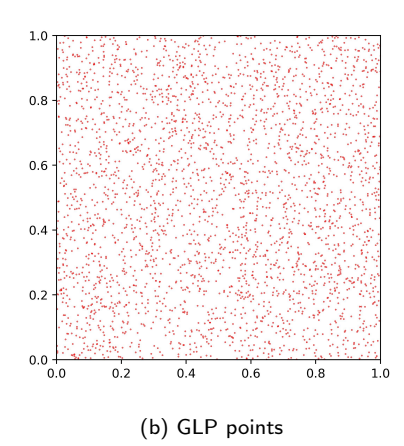
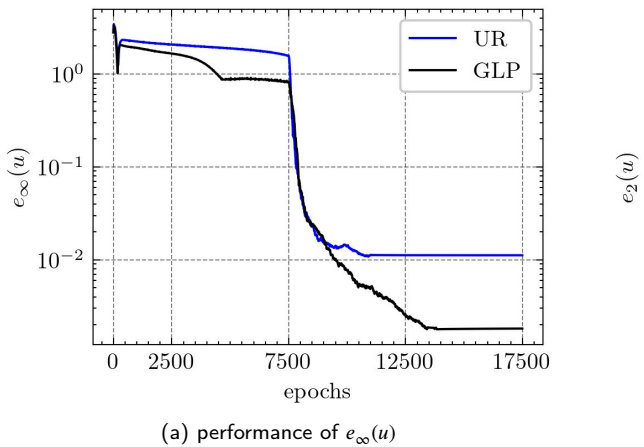


Figure 20: (a) the residual training points by uniform random sampling; (b) the residual training points by GLP set.

In Figure 21, we compare the numerical results derived from GLP set with those from uniform random sampling after 7500 epochs of Adam training and 10000 epochs of LBFGS training. This comparison aims to demonstrate the efficacy of our method for the same number of training points.



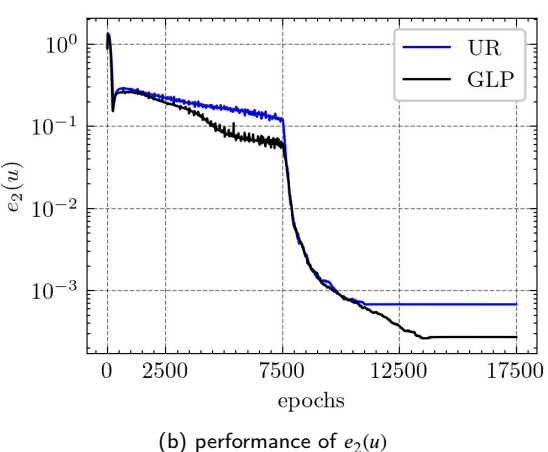


Figure 21: (a) the performance of relative error $e_{\infty}(u)$ during training process; (b) the performance of relative error $e_2(u)$ during training process.

Similar to the section 4.4, we also developed different training strategies by the number of training points and conducted controlled experiments with the GLP set. The specifics and outcomes of these different sampling strategies are comprehensively summarized in Table 7. The experimental results conclusively demonstrate that the GLP set possesses a clear advantage over uniform random sampling, even when the latter utilizes approximately five times the number of training points.

Table 7 The number of residual points in Ω and the number of boundary points at each hyperplane that composes $\partial\Omega$ under sampling strategies.

Strategy	1	2	3	4
Method	UR	UR	UR	GLP
Residual points	3001	5003	15019	3001
Each hyperplane	100	100	100	100
$e_2(u)$	6.813×10^{-4}	5.075×10^{-4}	4.027×10^{-4}	2.728×10^{-4}
$e_{\infty}(u)$	1.118×10^{-2}	3.669×10^{-3}	3.013×10^{-3}	1.818×10^{-3}

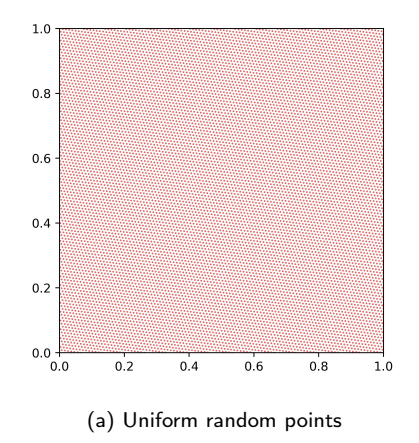
Table 8
The number of residual points in Ω and the number of boundary points at each hyperplane that composes $\partial\Omega$ under sampling strategies.

Strategy	1	2	3	4
Method	UR	UR	UR	GLP
Residual points	11215	24041	46213	11215
Each hyperplane	100	100	100	100
$e_2(u)$	1.020×10^{-3}	8.209×10^{-3}	5.680×10^{-3}	4.965×10^{-3}
$e_{\infty}(u)$	4.702×10^{-2}	4.330×10^{-2}	4.251×10^{-2}	1.512×10^{-3}

4.5.2. Eight-dimensional Problems

Here, we take d=8 and k=3 in Eq 51. And we sample 11215 points in Ω and 200 points in each hyperplane of $\partial\Omega$ as the training set and 500000 points as the test set. Moreover, we adjust the weights in the loss function so that $\alpha_1=10$ and $\alpha_2=1$. The other settings of main parameters in PINN are the same as Section 4.5.1.

Visualizing training points in the high-dimensional context poses a significant challenge, hence we restrict our plotting to the distribution of the first two dimensions for these 11215 residual training points, as depicted in Fig 22.



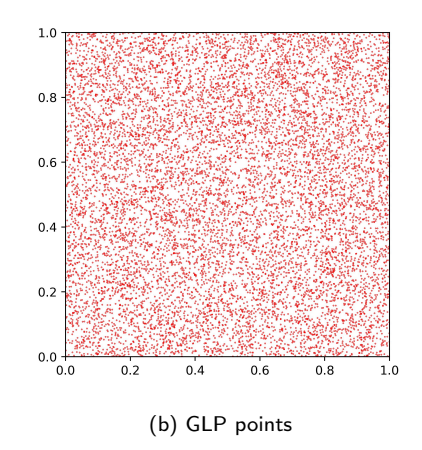


Figure 22: (a) the residual training points by uniform random sampling; (b) the residual training points by GLP set.

Figure 21, we compare the numerical results derived from GLP set with those from uniform random sampling after 20000 epochs of Adam training and 20000 epochs of LBFGS training. This comparison aims to show the effectiveness of our method for the same number of training points.

Similar to the section 4.4, we also developed different training strategies by the number of training points and conducted controlled experiments with the GLP set. The specifics and outcomes of these different sampling strategies are comprehensively summarized in Table 8. The experimental results conclusively demonstrate that the GLP set possesses a clear advantage over uniform random sampling, even when the latter utilizes approximately four times the number of training points.

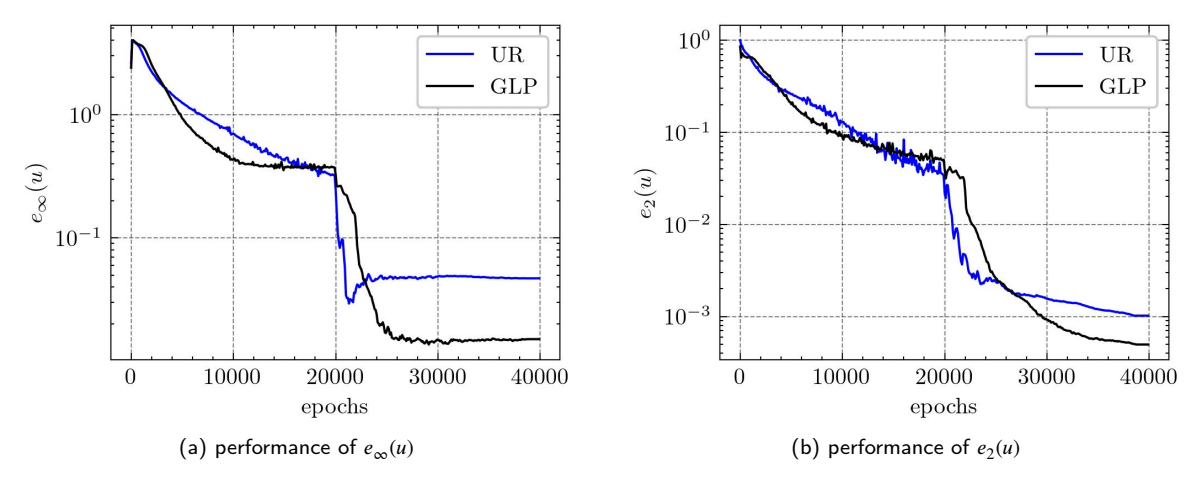


Figure 23: (a) the performance of relative error $e_{\infty}(u)$ during training process; (b) the performance of relative error $e_2(u)$ during training process.

5. Conclusions

This paper proposes utilizing good lattice points (GLP) set as sampling points to approximate the empirical loss function of Physics-Informed Neural Networks (PINN), aiming to reduce estimation errors. From a theoretical perspective, we prove the upper bound of the error for PINN based on the sampling method using GLP set. Additionally, we demonstrate that when using GLP set, the upper bound of the expected value of the squared error of PINN is smaller compared to using uniform random sampling. Numerical results based on our method, when addressing low-regularity and high-dimensional problems, indicate that GLP set outperforms traditional uniform random sampling in both accuracy and efficiency. In the future, we will do some work on how to use GLP set on other deep learning solvers and how to use number theoretic methods for non-uniform adaptive sampling.

Acknowledgment

This research is partially sponsored by the National Key R & D Program of China (No.2022YFE03040002) and the National Natural Science Foundation of China (No.12371434).

Additionally, we would also like to express my gratitude to Professor KaiTai Fang and Dr. Ping He from BNU-HKBU United International College for their valuable discussions and supports in this research.

References

- [1] Bottou, L., Curtis, F.E., Nocedal, J., 2018. Optimization methods for large-scale machine learning. SIAM review 60, 223-311.
- [2] Chen, J., Du, R., Li, P., Lyu, L., 2021. Quasi-monte carlo sampling for solving partial differential equations by deep neural networks. Numerical Mathematics 14, 377–404.
- [3] Fu, F., Wang, X., 2022. Convergence analysis of a quasi-monte carlo-based deep learning algorithm for solving partial differential equations. arXiv preprint arXiv:2210.16196.
- [4] Han, J., Jentzen, A., Weinan, E., 2018. Solving high-dimensional partial differential equations using deep learning. Proceedings of the National Academy of Sciences 115, 8505–8510.
- [5] Hlawka, E., 1961. Funktionen von beschränkter variatiou in der theorie der gleichverteilung. Annali di Matematica Pura ed Applicata 54, 325–333.
- [6] Keng, H.L., Yuan, W., 1981. Applications of number theory to numerical analysis. (No Title).
- [7] Kingma, D.P., Ba, J., 2014. Adam: A method for stochastic optimization. arXiv preprint arXiv:1412.6980.
- [8] Korobov, A., 1959a. The approximate computation of multiple integrals, in: Dokl. Akad. Nauk SSSR, pp. 1207–1210.
- [9] Korobov, N., 1959b. The evaluation of multiple integrals by method of optimal coefficients. Vestnik Moskovskogo universiteta 4, 19-25.
- [10] Li, Z., Kovachki, N., Azizzadenesheli, K., Liu, B., Bhattacharya, K., Stuart, A., Anandkumar, A., 2020. Fourier neural operator for parametric partial differential equations. arXiv preprint arXiv:2010.08895.
- [11] Liu, D.C., Nocedal, J., 1989. On the limited memory bfgs method for large scale optimization. Mathematical programming 45, 503-528.
- [12] Lu, L., Jin, P., Karniadakis, G.E., 2019. Deeponet: Learning nonlinear operators for identifying differential equations based on the universal approximation theorem of operators. arXiv preprint arXiv:1910.03193.
- [13] Lu, L., Meng, X., Mao, Z., Karniadakis, G.E., 2021. Deepxde: A deep learning library for solving differential equations. SIAM review 63, 208–228
- [14] Lyu, L., Wu, K., Du, R., Chen, J., 2020. Enforcing exact boundary and initial conditions in the deep mixed residual method. arXiv preprint arXiv:2008.01491.
- [15] Matsubara, T., Yaguchi, T., 2023. Good lattice training: Physics-informed neural networks accelerated by number theory. arXiv preprint arXiv:2307.13869.
- [16] Niederreiter, H., 1977. Pseudo-random numbers and optimal coefficients. Advances in Mathematics 26, 99-181.
- [17] Niederreiter, H., 1992. Random number generation and quasi-Monte Carlo methods. SIAM.
- [18] Raissi, M., Perdikaris, P., Karniadakis, G.E., 2019. Physics-informed neural networks: A deep learning framework for solving forward and inverse problems involving nonlinear partial differential equations. Journal of Computational physics 378, 686–707.
- [19] Renardy, M., Rogers, R.C., 2006. An introduction to partial differential equations. volume 13. Springer Science & Business Media.
- [20] Shin, Y., Darbon, J., Karniadakis, G.E., 2020. On the convergence and generalization of physics informed neural networks. arXiv e-prints, arXiv-2004.
- [21] Shin, Y., Zhang, Z., Karniadakis, G.E., 2023. Error estimates of residual minimization using neural networks for linear pdes. Journal of Machine Learning for Modeling and Computing 4.
- [22] Sirignano, J., Spiliopoulos, K., 2018. Dgm: A deep learning algorithm for solving partial differential equations. Journal of computational physics 375, 1339–1364.
- [23] Stein, M., 1987. Large sample properties of simulations using latin hypercube sampling. Technometrics, 143–151.
- [24] Tang, K., Wan, X., Liao, Q., 2020. Deep density estimation via invertible block-triangular mapping. Theoretical and Applied Mechanics Letters 10, 143–148.
- [25] Tang, K., Wan, X., Yang, C., 2023. Das-pinns: A deep adaptive sampling method for solving high-dimensional partial differential equations. Journal of Computational Physics 476, 111868.
- [26] Weinan, E., Yu, B., 2018. The deep ritz method: A deep learning-based numerical algorithm for solving variational problems. Communications in Mathematics and Statistics 6, 1–12.
- [27] Wu, C., Zhu, M., Tan, Q., Kartha, Y., Lu, L., 2023. A comprehensive study of non-adaptive and residual-based adaptive sampling for physics-informed neural networks. Computer Methods in Applied Mechanics and Engineering 403, 115671.
- [28] Yang, Q., Deng, Y., Yang, Y., He, Q., Zhang, S., 2023. Neural networks based on power method and inverse power method for solving linear eigenvalue problems. Computers & Mathematics with Applications 147, 14–24.
- [29] Yang, Y., Yang, Q., Deng, Y., He, Q., 2024. Moving sampling physics-informed neural networks induced by moving mesh pde. Neural Networks, 106706.